CHIMIKA CHRONIKA

NEW SERIES

AN INTERNATIONAL EDITION
OF THE ASSOCIATION OF GREEK CHEMISTS

CMCRCZ 26(1), 3-68(1997)

ISSN 0366-693X

1/97

Volume 26, No 1 p.p. 3-67 January-March 1997

CHIMIKA CHRONIKA

NEW SERIES

AN INTERNATIONAL EDITION

Published by the Association of Greek Chemists (A.G.C.)
27 Kaningos str. Athens 106 82 Greece
Tel. 00301-3821524 FAX: 00301-3833591

Correspondence, submission of papers, subscriptions, renewals and changes of address should be sent to Chimika Chronika-New Series, 27 Kaningos street, Athens 106 82, Greece. The Notice to Authors is published in the first issue of each volume, or sent by request. Subscriptions: 25 USD per year (individuals), 50 USD (libraries)

Phototypesetted and Printed in Greece by EPTALOFOS S.A.
12, Arditou Str. 116 36 ATHENS Tel. 9217.513

Υπεύθυνος σύμφωνα με το νόμο: Ν. Κατσαρός, Κάνιγγος 27, Αθήνα 106 82.

Responsible under law: N. Katsaros, 27 Kaningos St., Athens 106 82, Greece.

NOTICE TO AUTHORS

General Considerations

The international edition of *Chimika Chronika, New Series* invites original contributions on experimental and theoretical research and reviews in all branches of chemistry and related sciences at the molecular level.

All typescripts are subject to critical review. It is to be understood that the final decision relating to a typescript's suitability rests solely with the editors.

Special arrangements with the editors can sometimes be made in order to publish symposium articles as a group.

Typescripts should be written in English and a Greek summary should be included after the text. The Greek summary, headed by a Greek translation of the title, should be extensive and may refer to literature citations and tables or figures of the paper, in order to give a brief but factual account of the contents and conclusions of the article, and of its relevance; for this purpose, it may exceed half a printed page. In its place, foreign authors may submit an extensive summary in English, which will be gladly translated into Greek by care of the editors.

Types of Typescripts

Typescripts are classified as articles, short articles, letters, preliminary communications, notes and reviews.

Articles should cover their subjects with thoroughness, clarity, and completeness but should be as concise as possible. Articles are published in the order of acceptance within limitations of available space.

Short articles are concise but complete description of a small, rounded off investigation or of a side part from the main line of investigation, which will not be later included in an article.

Letters are short articles that report results whose immediate availability to the scientific community is deemed important. Letters often will be complete publications, but follow-up publication may occasionally be justified when the research is continued and a more complete account of work is deemed necessary.

Preliminary Communications are brief reports of results whose immediate availability to the scientific community is deemed important but which later will be included in an article. Although extensive references to the earlier literature usually are not needed, the most recent articles on the subject should be referred to, and sufficient experimental details should be given.

Notes are short articles on limited facets of an investigation e.g. describing a useful modification of an experimental technique or method, reporting additional data or more precise values for measurements already existing in the literature etc.

Reviews should be fully comprehensive on a narrow field of specialized research, expected to be interesting for a great number of scientists; they are invited articles, otherwise submitted after contacting the editors.

Submission of Typescripts

Typescripts should be submitted in triplicate to **P.N. Dimotakis, Editor-in-Chief, *Chimika Chronika, New Series*, Association of Greek Chemists, 27 Kaningos Street, GR-106 82 ATHENS, GREECE.**

Authors are encouraged to include their FAX number in the cover letter.

Preparation of Typescripts for Direct Reproduction

Papers will normally be published from Author-prepared camera-ready typescripts. Typescripts should be on goodquality white A4 size paper; they will normally be reproduced after photographic reduction to 82% the original size. To ensure that, after reduction, the

area of typescript is suitable for page-size of the published journal Authors should take special care that all figures and text are within a typing- or image-area of 212 mm height (225 mm when the running title is included) and 151 mm width.

Ideally typescripts should be laser printed. Typesscripts should be typed in a single-column layout leaving equal space from both sides, using Elite Times Roman font. References should be indicated by using arabic numerals in square brackets.

First page: Leave 47 mm space and then type the Article title full left, in 14pt bold, all in capital letters. Leave triple space and type the Author name(s) (in bold) and addresses on separate lines (1 1/2 line spacing) full left, in 12pt, capitalizing the first letter of all main words. Use an asterisk to identify the corresponding Author. Leave fivefold space and type the Abstract (single line spacing) full left to the full width, without a heading. Leave double space and type Key Words. Leave triple space and type the Section heading (Introduction) in 12pt bold, capitalizing the first letter. Section headings and subheadings (and Table...) should be typed full left. Do not underline the headings and leave double space between all headings and the paragraphs which precede and follow them. Type the text (1 1/2 line spacing). Each new paragraph should start indended 5 spaces, and only 1 1/2 spaced from the preceding paragraph.

All other pages: Leave 32 mm space and then type the Author name(s) in 12pt, capitalizing the first letter of all main words, over to the right for even-numbered pages, and the Article title in 12pt, all in capital letters, over to the left for odd-numbered pages. Leave triple space and continue typing the text.

Insofar as possible Authors should use systematic names similar to those used by the International Union of Pure and Applied Chemistry and the Chemical Abstracts. SI units and symbols should be used.

Acknowledgement should be typed full left, followed by a dash and by the acknowledgement statement itself.

A character size of 12pt and single line spacing should be used. Journal articles and books must be cited by the following formats:

1. Valavanidis, A; Gilbert, B.C.; Whitwood, A.C. Chimika Chronika, New Series 1995, 24, 217-232.

2. Cross, A.D.; Jones, R.A. Introduction to Practical InfraRed Spectroscopy, 3rd ed.; Plenum: New York, 1969; Chapter 2.

Typescript for Short Articles and Preliminary Communications should be organized on the same principles. Besides some minor modifications in their published form, they differ from an article in that the headings and subheadings in the text, as well as the abstract preceeding the text are ommitted. In these cases, the first paragraph of the text may serve the purpose of an abstract, summing up very briefly the scope and the main findings and conclusions of the investigations.

Direct reproduction of camera-ready articles requires the author to provide the typescript in a finished artistic format, making the best possible use of the space **within an even number of completely utilized pages** which should be numbered lightly in pencil. All figures (the word Figure... should be written in full) must be inserted within the camera-ready text (should pasted in place, not taped). Please remember that the lettering on figures should be of appropiate size for reproduction after reduction. Tables and formulas should be placed appropriately within the typescript. Formulas and other graphical material should be drawn with special care and pasted up exactly as the page is to appear in the journal. Editors may return otherwise acceptable articles for modification if the quality of the figures or formulas is poor or the overall layout is carelessly composed.

Where these suggestions for format at type size cannot be followed in detail, authors should primarily ensure that they keep as closely as possible to the measurements given above for the image area of a page.

Page Charge and reprints: 2.000 Drachmas or 10 USD for 25 reprints (upon request).

Chimika Chronika, New Series, 26, 3-18 (1997)

IONIZATION ENERGIES OF MOLECULES

Ana Medved

Department of General and Inorganic Chemistry, Faculty of Chemical Engineering and Technology, University of Zagreb

(Received: January 3, 1996 In final form: September 10, 1996)

SUMMARY

This work deals with the extended theory of BOHR, and especially with the calculation of ionization energies of molecules. New formulae have been derived, based upon the frequency rule of BOHR, and their applicability shown upon several examples chosen from inorganic and organic compound.

INTRODUCTION

Among other characteristic properties of molecules, the energies of ionization can reflect their structure and enable the comparison of bond strengths. The ease of involving the outermost electrons in bonding, coupled with the higher second stage ionization energies can explain the predominant covalency of the bond or its partially ionic character. The proportion of resonant structures can also be indicated by energies of ionization. The scope of investigating energies of ionization is great and heplful in many fields of the chemical science. Therefore a new theory which enables the theoretical calculation of ionization energies is of a significant practical use.

However, it is the intention of this work also to show the advantages of the corpuscular theory based upon the principles of classical mechanics. The accuracy, the ease of calculation and the visualization of the corpuscular systems are inspiring creativity of organic and inorganic chemists and even of physicistsand induce a sense of mastering the understanding of the interdependance of the movements of subatomic particles.

THEORY

1. Surface ionization of molecules

The corpuscular theory approach for calculating ionization energies is applying the simple rules set up for atomic shielding constants to atoms in molecules as well, because the atoms preserve their basic properties if they form molecules, but the shielding constants for the bonding electrons differ and had to be established in this work. Variation of the shielding constants appeared to be necessary also for hybridized electrons and electrons from the neighbouring atoms as well.

Therefore a formula derived in the previous work[1] for ionization energies of atoms:

$$IE = 13.6 \cdot (Z-s) \cdot \left\{ \frac{1}{n^2 \pm m_l + m_s} \right\} \qquad (1)$$

was developed for the application upon molecules, by the introduction of shielding constants for bonding electrons.

I. TABLE OF SHIELDING CONSTANTS FOR MOLECULES

Bonding mode	Shielding constants
σ- bond	0.20
π- bond	0.15
hybridized electrons	0.15
electrons from the neighbouring atoms	0.15

In the above formula where: (Z-s) = effective nuclear charge
s = shielding constants
n = principal quantum number
m_l = orbital magnetic quantum number
m_s = spin quantum number

the parameters in the denominator are pertaining to repulsive forces of unpaired electrons. Thus the formula is constituted for a seemingly diparticle system with a shielded nuclear charge and a decreased electronic charge.

Accordingly, the shielding constants and the parameters in the denominator are enabling a polyparticle system to be mathematically translated into a diparticle system.

2. Inner ionization (core ionization)

For the release fo inner electrons (X-ray photoelectron spectroscopy (XPS)) a new formula had to be derived:

$$IE = 13.6 \cdot (Z-s) \cdot \left\{ \frac{1}{n \pm m_l + m_s} \right\} \qquad (2)$$

where the notations have the same significance as those in the first formula. The derivation by the simple algebraic approach constituting the theory of BOHR is better suitted for the chemical visualization of matter than the operators applied by physicists and mathematicians in wave-mechanics for calculating relativistic ionization energies[2] , and even the accuracy is better than that achieved by the differential equations.

Accordingly, the derivation begins with the sum of the kinetic and potential energy, after BOHR:

$$E_{(p+k)} = -\frac{1}{2} \cdot \frac{Ze^2}{r} \qquad (3)$$

Such formula becomes applicable for ionization, when the condition of a single outer electron is introduced, i.e. Z = 1

$$IE = +\frac{1}{2} \cdot \frac{e^2}{r} \qquad (4)$$

For inner ionization a second condition must be introduced, i.e. n = 1. By inserting the radius with such a condition into equation (4), the inner ionization formula is resulting:

$$IE = \frac{2^2 . m . Z . e^4}{1 \cdot h^2} = 13.6 \cdot Z \text{ eV} \qquad (5)$$

For polyelectronic systems (atoms and molecules) the above formula is

supplemented by variable parameters pertaining to effects of shielded nuclear charge and the repulsive forces between the electrons in the shells[1-4] :

$$IE = 13.6 \cdot \left\{ \frac{(Z-s)}{n \pm m_l + m_s} \right\} \qquad (6)$$

When taking into account the condition introduced in the derivation of the radius, i.e. the quantum number n = 1, the equation (6) is resulting but containing $\underline{n}$ not as a dynamical variable, but n inserted as a parameter encompassing the repulsive forces.

APPLICATION AND RESULTS

The above formulae and the corresponding shielding constants have been applied for calculating the ionization energies of molecules involving different types of bonding, σ and π , including the substituents, and the metallic and ionic bonds as well. A theoretical and stereochemical interest is attached often to assignments of maxima especially by electron spectroscopists. The maxima measured by such experimental technique can be unambiguously assigned by calculating the corresponding energies of ionization. Therefore, the spectra registered by the electron spectroscopic technique have been used to show the "best fit" procedure of the calculation. The compounds ethene, vinyl fluoride, and benzene have been chosen among organic compounds from reference[5], and gold, sodium chloride, argon, xenon, platinum as well as graphite, N_2 and O_2 from reference Siegbahn et al. ESCA[6] .

ETHENE

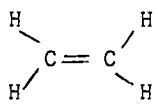

a) Release of a π-electron:

The π-electron released consumes the ionization energy of an electron

on a carbon atom:

$$(Z\text{-}s) = 6 - 2 \cdot 0{,}75 - 3 \cdot 0{,}15 - 4 \cdot 0{,}15 = 3{,}45$$

(hybridized)

$$IE = 13.6 \cdot (Z\text{-}s) \cdot \left\{ \frac{1}{n^2 \pm m_l + m_s} \right\}$$

$$IE = 13.6 \cdot 3{,}45 \cdot \left\{ \frac{1}{2^2 \pm 0 + 0{,}5} \right\} = 10{,}43 \text{ eV}$$

(measured 10,51 eV)[5]

2s 2p

Thereby there are 4 electrons from the neighbouring atoms considered to be in the sphere of the carbon atom (s = 4 . 0,15).

VINYL FLUORIDE

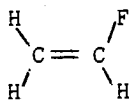

a) The π-electron released when the other electrons from the neighbouring atoms are considered to be in the sphere of the calculated C-atom:

$$(Z\text{-}s) = 6 - 2 \cdot 0{,}75 - 3 \cdot 0{,}15 - 3 \cdot 0{,}15 - 0{,}15 = 3{,}45$$

$$IE = 13.6 \cdot \frac{3{,}45}{4{,}5} = 10{,}43 \text{ eV} \qquad \text{(measured 10,37 eV)}[5]$$

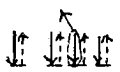

2s 2p

In the next examples the unpaired electron remaining after ionization is in the neighbouring atom. Its $m_s = 0{,}5$ is not to be taken into acount in the calculation.

b) The σ-electron from the C-atom released when the electrons are in the neighbouring atoms:

$$(Z\text{-}S) = 6 - 2 \cdot 0{,}75 - 2 \cdot 0{,}2 - 0{,}15 = 3{,}95$$

$$IE = 13.6 \cdot \frac{3{,}95}{3} = 18{,}0 \text{ eV} \quad (\text{measured } 18{,}0 \text{ eV})^5$$

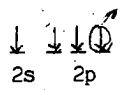

c) The σ-electron released at the moment when one electron from the neighbouring atom is in the sphere of the emitting atom.

$$(Z\text{-}s) = 6 - 2 \cdot 0{,}75 - 4 \cdot 0{,}15 = 3{,}9$$

$$IE = 13.6 \cdot \left\{ \frac{3{,}9}{4 + 1 + 0} \right\} = 10{,}60 \text{ eV} \quad (\text{measured } 10{,}6 \text{ eV})^5$$

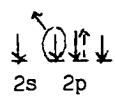

d) The σ-electron released when 2 other electrons are in the sphere of the considered C-atom:

$$(Z\text{-}s) = 6 - 2 \cdot 0{,}75 - 4 \cdot 0{,}15 - 0{,}2 = 3{,}70$$

$$IE = 13.6 \cdot \frac{3{,}70}{3} = 16.73 \text{ eV} \quad (\text{measured } 16{,}73 \text{ eV})^5$$

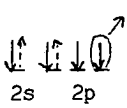

e) The first ionization from a free electronic pair upon fluorine:

$$(Z\text{-}s) = 9 - 2 \cdot 0{,}7 - 6 \cdot 0{,}15 = 6{,}7$$

$$IE = 13.6 \cdot \left\{ \frac{6{,}7}{4 + 0 + 0{,}5} \right\} = 20{,}30 \text{ eV} \quad (\text{measured } 20{,}4 \text{ eV})^5$$

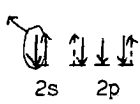

BENZENE

The aromatic compounds containing hybridized and nonhybridized σ-and π-bonds are emitting a wide variety of spectral systems. A gradation of the ionization energies is observable, paralleling the orientation of the orbitals in the magnetic field:

a) $(Z-s) = 6 - 2 \cdot 0{,}75 - 3 \cdot 0{,}2 - 0{,}15 = 3{,}75$

$$IE = 13{,}6 \cdot 3{,}75 \cdot \left\{ \frac{1}{4 + 1 + 0{,}5} \right\} = 9{,}27 \text{ eV (measured } 9{,}3)^5$$

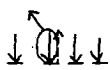

b) $(Z-s) = 6 - 2 \cdot 0{,}75 - 3 \cdot 0{,}2 - 0{,}15 = 3{,}75$

$$IE = 13{,}6 \cdot 3{,}75 \cdot \left\{ \frac{1}{4 + 0 + 0{,}5} \right\} = 11{,}33 \text{ eV (measured } 11{,}3)^5$$

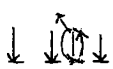

c) $(Z-s) = 6 - 2 \cdot 0{,}75 - 0{,}2 - 4 \cdot 0{,}15 = 3{,}7$

$$IE = 13{,}6 \cdot 3{,}7 \cdot \left\{ \frac{1}{4 - 1 + 0} \right\} = 16{,}77 \text{ eV (measured } 16{,}8)^5$$

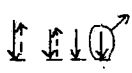

SODIUM CHLORIDE

a) Another point of defference is shown by the example of electron emission from the 2nd energy level of an ion Na^+:

$$(Z\text{-}s) = 11 - 2 \cdot 0{,}75 - 7 \cdot 0{,}2 = 8{,}1$$

$$IE = 13{,}6 \cdot 8{,}1 \cdot \left\{ \frac{1}{2 + 1 + 0{,}5} \right\} = 31{,}4 \text{ eV}$$

(measured 31,0 eV)[6]

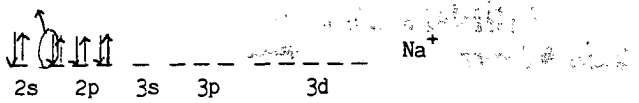

b) The electron emision from the chloride ion is consistent with an unexpected sequence in the orbitals. It suggests a substantial polar stability of the ionic bond. This example is showing spin-orbital splitting.

$$(Z\text{-}s) = 17 - 2 - 8 \cdot 0{,}75 - 5 \cdot 0{,}2 - 2 \cdot 0{,}75 = 6{,}5$$

nonhybridized

$$IE = 13{,}6 \cdot 6{,}5 \cdot \left\{ \frac{1}{9 + 4{,}0 + 3 \cdot 0{,}5} \right\} = 6{,}09 \text{ eV}$$

(measured 6,0 eV)[6]

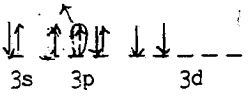

c) There is a second maximum displayed at 16,8 eV and the calculations have indicated an emission from the p-orbital, accompained by a different spin-orbit splitting:

$$(Z\text{-}s) = 17 - 2 - 8 \cdot 0{,}75 - 7 \cdot 0{,}15 = 7{,}95$$ hybridized

$$IE = 13{,}6 \cdot 7{,}95 \cdot \left\{ \frac{1}{9 - 2 - 1 - 1 + 3 \cdot 0{,}5} \right\} = 16{,}63 \text{ eV}$$

(measured 16,7 eV)[6]

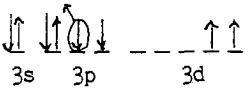

POTASSIUM HEXACHLORO PLATINATE

$K_2 \left[PtCl_6\right]$

The assignment of the maximum arising when the emitted electron comes from the inner orbitals of Pt (4. energy level) is very exact, when the core ionization calculations are applied. The formula (2) for core ionization is used.

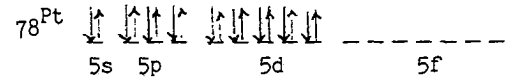

(The configuration of Pt^0)

$$(Z-s) = 78-2-8-18-17 \cdot 0{,}4-14 \cdot 0{,}55-14 \cdot 0{,}35-6 \cdot 0{,}15 = 29{,}7$$

$$IE = 13{,}6 \cdot 29{,}7 \cdot \left\{ \frac{1}{4+1+0{,}5} \right\} = 73{,}44 \text{ eV}$$

(measured 73,4 eV)[6]

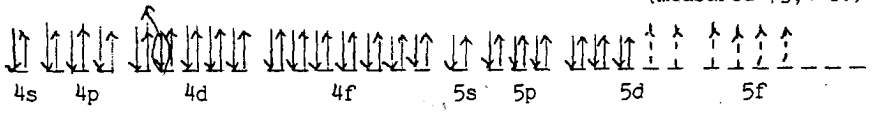

From d-orbitals electrons are also emitted from noncomplex platinum ion, indicating a dissociated structure:

$$(Z-s) = 78-2-8-18-17 \cdot 0{,}4-13 \cdot 0{,}55-14 \cdot 0{,}35-0{,}2 = 30{,}95$$

$$IE = 13{,}6 \cdot 30{,}95 \cdot \left\{ \frac{1}{4+1+0{,}5} \right\} = 76{,}57 \text{ eV}$$

(measured 76,6)[6]

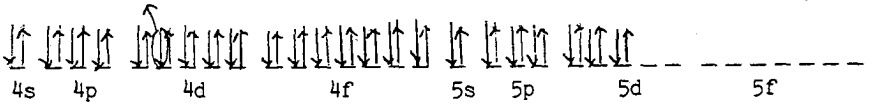

GOLD

The spectra of gold, registered by electron spectroscopy displayed in reference (6), have been used for the "best fit" procedure.

a) The emission of the 5f-electron from Au:

$$(Z\text{-}s) = 79 - 2 - 8 - 18 - 32 \cdot 0{,}9 - 18 \cdot 0{,}9 = 6{,}0$$

$$IE = 13{,}6 \cdot 6{,}0 \cdot \left\{ \frac{1}{25 + 0 + 0} \right\} = 3{,}26 \text{ eV}$$

(measured 3,2 eV)[6]

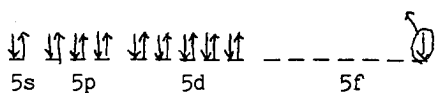

b) The peak resulting when the electrons in the close packed fcc metallic structure are forming bonds[7]:

$$(Z\text{-}s) = 79 - 2 - 8 - 18 - 32 \cdot 0{,}9 - 12 \cdot 0{,}9 - 6 \cdot 0{,}2 = 10{,}2$$

$$IE = 13{,}6 \cdot 10{,}2 \cdot \left\{ \frac{1}{25 + 0 + 0} \right\} = 5{,}55 \text{ eV}$$

(measured 5,5 eV)[6]

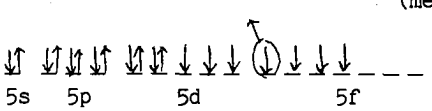

The spectrograms of gold comprise also the inner electron emission maxima registered with XPS, as the authors of reference (6) have shown. The attempt to asign them by the formula derived previously is shown next:

c) When electrons are emitted from 4f-orbitals:

$$(Z\text{-}s) = 79 - 2 - 8 - 18 - 18 \cdot 1 - 13 \cdot 0{,}55 - 18 \cdot 0{,}9 - 0{,}2 - 0{,}15 = 9{,}3$$

$$IE = 13{,}6 \cdot 9{,}3 \cdot \left\{ \frac{1}{4 - 3 + 0{,}5} \right\} = 84{,}32 \text{ eV}$$

(measured 84,0 eV)[6]

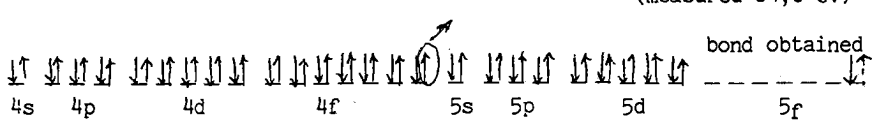

d) $(Z-s) = 79 - 2 - 8 - 18 - 18 \cdot 1 - 13 \cdot 0{,}55 - 19 \cdot 0{,}35 = 19{,}2$

$$IE = 13{,}6 \cdot 19{,}2 \cdot \left\{ \frac{1}{4 - 2 + 2 \cdot 0{,}5} \right\} = 87{,}04 \text{ eV}$$

(measured 87,1 eV)[6]

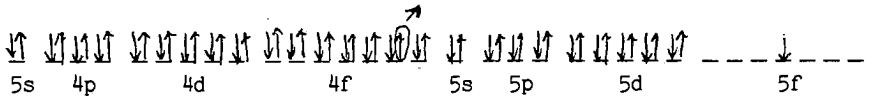

ARGON

Because the most probable emission of an electron is the magnetically favorable[1] , the atom is tending to adopt a conducive configuration by spin-orbit splitting, whereby the symmetry effects are also implied. The example of argon is showing the splitting od an 3p and 3s electronic pair, with ionization resulting in two ionic states. Therefore 2 maxima are formed with an intensity ratio 2:1, the first at 15,76 eV and the second at 15,93 eV[6]. The corresponding configuration interactions are:

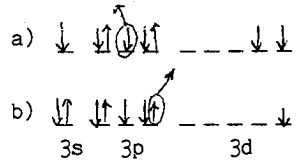

a) $(Z-s) = 18 - 2 - 8 \cdot 0{,}75 - 5 \cdot 0{,}2 - 2 \cdot 0{,}15 = 8{,}7$

b) $(Z-s) = 18 - 2 - 8 \cdot 0{,}75 - 3 \cdot 0{,}2 - 4 \cdot 0{,}15 = 8{,}8$

a) $$IE = 13{,}6 \cdot 8{,}7 \cdot \left\{ \frac{1}{9 - 3 + 1{,}5} \right\} = 15{,}77 \text{ eV}$$

(measured 15,75 eV)[6]

b) $$IE = 13{,}6 \cdot 8{,}8 \cdot \left\{ \frac{1}{9 - 3 + 1{,}5} \right\} = 15{,}91 \text{ eV}$$

(measured 15,93 eV)6

XENON

Xenon does emit electrons from d-orbitals and the emission is paralleled by two spin-orbit splittings in the ratio 2:1[6] . This maxima were calculated by the formula (1) for surface ionization:

a) $(Z-s) = 54 - 2 - 8 - 18 - 16 \cdot 0{,}4 - 9 \cdot 0{,}55 = 14{,}65$

$$IE = 13{,}6 \cdot 14{,}65 \cdot \left\{ \frac{1}{16 - 0 + 0{,}5} \right\} = 12{,}10 \text{ eV}$$

(measured 12,12 eV)[6]

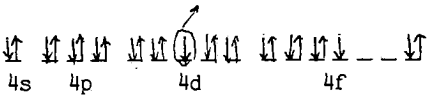

b) $(Z-s) = 54 - 2 - 8 - 18 - 14 \cdot 0{,}4 - 11 \cdot 0{,}55 = 14{,}35$

$$IE = 13{,}6 \cdot 14{,}35 \cdot \left\{ \frac{1}{16 - 2 + 0{,}5} \right\} = 13{,}42 \text{ eV}$$

(measured 13,43 eV)[6]

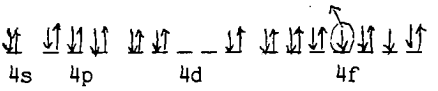

The XPS induced ionization of Xe from the 3. energy level is fitting with the p-orbital electron emission, but accompanied by a spin-orbit splitting in the uper level. The formula (2) was used for inner ionization.

$$(Z-s) = 54 - 2 - 8 \cdot 0{,}75 - 7 \cdot 0{,}2 - 10 \cdot 0{,}75 - 17 - 9 \cdot 0{,}55 = 15{,}15$$

$$IE = 13{,}6 \cdot 15{,}15 \cdot \left\{ \frac{1}{3 - 3 + 2 \cdot 0{,}5} \right\} = 206{,}0 \text{ eV}$$

(measured 206,0 eV)[6]

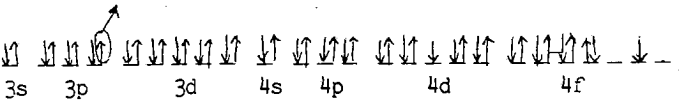

Data from reference (6) which were used for comparison with the calculated values, give a description of the preparation of the samples of noble gases for XPS measurements. The Xe ions were reduced at a metalic foil electrode and deposited upon it as a thin layer of atoms. As a consequence the attached atoms formed still a bondage with the metallic foil. This fact is theoretically observable in the calculation with 2 unpaired electrons, the third being paired upon the metal.

3. Inner ionization formula for the elements of the second energy level

For inner ionization calculations of the second row elements an exceptional formula (7) is requested, because the electron released from the 1s orbital of such elements must penetrate an envelope of symmetrically arranged 2 - 8 electrons. The empirically established accordance with the formula indicates an independance of the ionization energy upon the orientation of the enveloping electronic cloud in the magnetic field, but a dependance upon the number of the enveloping electrons. Accordingly the number of electrons is also a parameter applicable for the calculation of ionization energies, consistent with the size of the interspace trough which the emitted electron is penetrating, counteracting the repulsive forces.
The formula (7)

$$IE = 13{,}6 \cdot (Z\text{-}s) \cdot \frac{1}{1/a} \qquad (7)$$

where a = number of electrons in the enveloping 2. energy level
was applied to several molecules for verification.

GRAPHITE

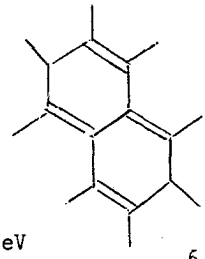

a) Surface ionization:

$$(Z\text{-}s) = 6 - 2 \cdot 0{,}75 - 3 \cdot 0{,}15 = 4{,}05$$

$$IE = 13{,}6 \cdot 4{,}05 \cdot \left\{ \frac{1}{4 - 1 + 0} \right\} = 18{,}36 \text{ eV}$$

(measured 18,34 eV)[6]

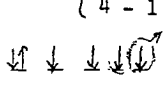

1s 2s 2p

b) Inner ionization:

$$(Z\text{-}s) = 6 - 0{,}2 - 4 \cdot 0{,}15 = 5{,}20$$

$$IE = 13{,}6 \cdot 5{,}20 \cdot \frac{1}{1/4} = 282{,}9 \text{ ev}$$

(measured 284,0 eV)[6]

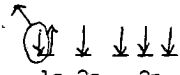

NITROGEN $|N \equiv N|$

a) $(Z\text{-}s) = 7 - 2 \cdot 0{,}70 - 2 \cdot 0{,}2 - 2 \cdot 0{,}15 = 4{,}90$

$$IE = 13{,}6 \cdot 4{,}9 \cdot \left\{ \frac{1}{4 + 0 + 0} \right\} = 16{,}65 \text{ eV}$$

(measured 16,7 eV)[6]

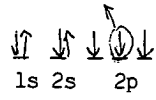

b) $(Z\text{-}s) = 7 - 0{,}2 - 3 \cdot 0{,}2 - 2 \cdot 0{,}15 = 5{,}90$

$$IE = 13{,}6 \cdot 5{,}90 \cdot \frac{1}{1/5} = 401{,}2 \text{ eV}$$

(measured 402 eV)[6]

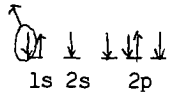

OXYGEN $|\bar{O} \equiv \underline{O}|$

a) $(Z\text{-}s) = 8 - 2 \cdot 0{,}75 - 4 \cdot 0{,}2 - 0{,}2 = 5{,}5$

$$IE = 13{,}6 \cdot 5{,}5 \cdot \left\{ \frac{1}{4 - 1 - 0} \right\} = 24{,}9 \text{ eV}$$

(measured 24,9 eV)[6]

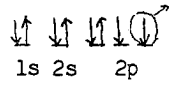

b) $(Z\text{-}s) = 8 - 0{,}2 - 5 \cdot 0{,}2 - 0{,}15 = 6{,}5$

$$IE = 13{,}6 \cdot 6{,}5 \cdot \frac{1}{1/6} = 530{,}4 \text{ eV}$$

(measured 532 eV)[6]

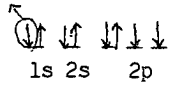

II. TABLE OF SHIELDING CONSTANTS

Electrons on the same energy level:

s and p electrons are contributing upon all energy levels			0.20
d -electrons with all electrons in the	3.	level	0.75
- " -	4.	level	0.40
- " -	5.	level	0.20
f^{1-8}-electrons with all electrons in the	4.	level	0.55
- " -	5.	level	0.35
f^{9-14}-electrons with electrons f^{1-14} of the	4.	level	0.55
and with the s, p, d-electrons			1.00
f^{9-14}-electrons of the	5.	level	0.35
and with the s, p, d, f^{1-8}-electrons			0.90

Electrons on the level underneath:

Electrons under s-orbitals of the	1.,2.,3.	level	0.70
Electrons under p-orbitals of the	1.,2.,3.	level	0.75
Electrons under s and p-orbitals of the	6.	level	0.55
Electrons under s and p-orbitals of the	5.	level	0.75
Electrons under d and f-orbitals of the	3.,4.	level	1.00
Electrons under d and f-orbitals of the	5	level	0.90
Electrons in the lower levels			1.00

The sequence of quantum numbers is regular: 1, 2, 3, 4, 5 and not 3.7 or 4.2 as with SLATER's modified quantum numbers.

ΕΝΕΡΓΕΙΕΣ ΙΟΝΤΙΣΜΟΥ ΜΟΡΙΩΝ

Η παρούσα εργασία αναφέρεται στην εκτεταμένη θεωρία του Bohr και ειδικότερα στον υπολογισμό της ενέργειας ιοντισμού των μορίων. Εχουν παραχθεί νέοι τύποι, που βασίζονται στον κανόνα συχνότητας του Bohr και των οποίων η εφαρμογή καταδεικνύεται μέσω παραδειγμάτων επιλεγμένων από οργανικές και ανόργανες ενώσεις.

REFERENCES

1. A. MEDVED: "Ionization Energies, Calculated by a new Formula", XIII. Meeting of Croatian Chemists, Zagreb 1993.

2. G. NARAY-SZABO, P.R. SURJAN and J.G. ANGYAN: "Applied Quantum Chemistry" Akademiai Kiado, Budapest, (1987).

3. J. C. SLATER: The Physical Review, Vol. 36, (1930)

4. C. W. N. CUMPER: "Wave Mechanics for Chemists", Heinemann Educational Books, London 1966, pp. 118,119.

5. L. KLASINC, B. KOVAČ i B. RUŠČIĆ: Kem. Ind. (1974), 10, 569.

6. K. SIEGBAHN et AL. "ESCA of Free Atoms and Molecules", North-Holland, 1970, Amsterdam.

7. T. KOOPMANS: Physica, 1 (1934) 104.

Chimika Chronika, New Series, 26, 19-28 (1997)

MICROANALYSIS OF COATINGS.

E. Valamontes

Institute of Microelectronics, NRCPS "Demokritos", P.O. Box 60228, 153 10 Aghia Paraskevi, Attiki, Greece.

(Received: October 2, 1996 In final form: November 12, 1996)

Monte-Carlo simulations have been applied to Electron Probe X-ray Microanalysis of thin coatings on a bulk material. The X-ray signal from the film and its lateral extent as a function of film thickness, primary beam energy and angle of incidence were calculated. All contributions to the measured total X-ray signal were taken into account. These are:
a) The signal induced by the primary electron beam.
b) The signal induced by backscattering, considered both within the film and the substrate.
c) The signal induced by characteristic and continuous X-rays, created within the substrate by incident and backscattered electrons, which ionise the atoms of the film in their way out of it.

KEY WORDS: EPMA, Coatings, Monte-Carlo.

INTRODUCTION

Electron Probe X-ray Microanalysis (EPMA) is a well known and established technique for the quantitative analysis of bulk materials [1-4]. The formalism used is applied to samples which are homogeneous in composition in the whole analysed volume. But when the analysed elements are not homogeneously distributed in the sample, as in the case of small inclusions in a different matrix or stratified materials, the formalism used for bulk materials is no longer valid and different approaches are needed. The first attempts to apply EPMA to the analysis of stratified materials were based on the determination, of the $\varphi(\rho z)$ function, giving the distribution of the generated X-ray signal as a function of depth (Philibert et al. [5], Reuter [6] and Brown [7]). This approach is quite complicated and several assumptions were needed. Monte-Carlo simulations

were also used (Bishop and Poole [8], Kyser and Murata [9], Foulu and Henoc [10]), but also with important simplifications, in order to reduce computer time. A more elaborated model was that of Pouchou and Pichoir [11-13] which constitutes an analytical model established by considering both general laws and Monte-Carlo simulations in order to obtain the φ(pz) curve of stratified materials as a function of primary beam energy. The chemical composition and film thickness of the analysed samples are obtained by measuring experimentally the ratio of intensities of the analysed element from the sample and from a standard of known and homogeneous composition, containing the same element.

A simplified model, applied in the case of coatings which are sufficiently thin compared to the corresponding electron range (thickness t $\leq R_e/10$, R_e=electon range) was that of Cazaux et al. [14-15], based on a formalism analogous to that applied in Auger Electron Spectroscopy. In this formalism, the X-ray signal emitted by element A of a film of thickness t on a substrate B is written as:

$$I_{A/B} = C_A . \rho . \left(\frac{N}{A}\right) . I_p . \omega_{ij} . \sigma_X^A (E_0) . (1+T_{A/B}) . t . T$$

where C_A is the concentration of element A in the film, p is the volume density and A the atomic mass, N is Avogadro's number, I_p (in e^-/sec) is the primary beam current, ω_{ij} the fluorescence yield, $\sigma_X^A (E_0)$ the ionisation cross section by electrons of energy E_0, T is the collection efficiency and $T_{A/B}$ is a total correction factor taking into account all ionisations within the substrate (backscattered electrons and X-rays created within the substrate, which ionise the atoms of the film). Only characteristic X-rays from the substrate are in general taken into account. Nassiopoulos and Valamontes [16-18] and Valamontes et al. [19] made more exact calculations of the correction factor $T_{A/B}$, by including also fluorescence from continuous X-rays created within the substrate. They used Monte-Carlo simulations for these calculations and they found that in some cases (high primary beam energy and substrate of a high Z material) the contribution from continuous X-rays is very important and not negligible. The

factor $T_{A/B}$ was also measured experimentally by this group [17] and by Cazaux et al. [14], by measuring under the same conditions the X-ray signal of element A from the film on a substrate B and the signal from a thin unsupported film of the same thickness and by calculating the ratio of these two signals. The signal from the thin unsupported film is equal to the signal due to the primary beam.

In the present work, the above calculations are extended to the case where the film is not thin, compared to the electron range. Backscattering within the film is in this case taken into account and the change of the ratio I_{total}/I_{film} with film thickness as a function of primary beam energy and angle of incidence will be discussed.

The radial distribution of the X-ray signal from the film is also calculated in this work for different film thicknesses and angles of incidence. The corresponding Monte-Carlo programme is quite general and takes into account all contributions to the total signal, as described above. But even though the Monte-Carlo programme is quite complicated, it can be run on a personal computer.

RESULTS AND DISCUSSION

The Monte-Carlo programme has been described in detail elsewhere [16]. The incident electron beam is normally distributed (gaussian curve) around the point of incidence, with a standard deviation $\sigma_0=40\,\text{Å}$. For each incident electron the electron trajectory within the sample (including both the film and the substrate) is first calculated. Backscattering within both the film and the substrate is considered. The X-ray signal from the film is then calculated for the part of electron trajectory, situated within the film. Fluorescence from characteristic X-rays is considered in the following way: the created characteristic X-rays along the electron path which have enough energy, ionise the analysed atoms from the film with a probability given by the X-ray ionisation cross section at the corresponding energy. A random number determines the emission angle of these X-rays which produce the signal of interest in their way out of the sample.

Fluorescence due to continuous X-rays is calculated as described in reference [16]. Only continuous X-rays from the substrate are taken into account.

An example of application of the Monte-Carlo programme is given in Fig. 1 which shows the total X-ray signal from a copper film on a gold substrate as a function of primary beam energies, in the range 10-50 keV. The film thicknesses are between 40nm and 400nm. The analysed line is CuKa. The total signal is normalised to the signal from an unsupported film of the same thickness, calculated separately. The contribution of the substrate is thus separated from the signal generated directly within the film by the incident beam. As expected, this contribution is more important when the film is thin.

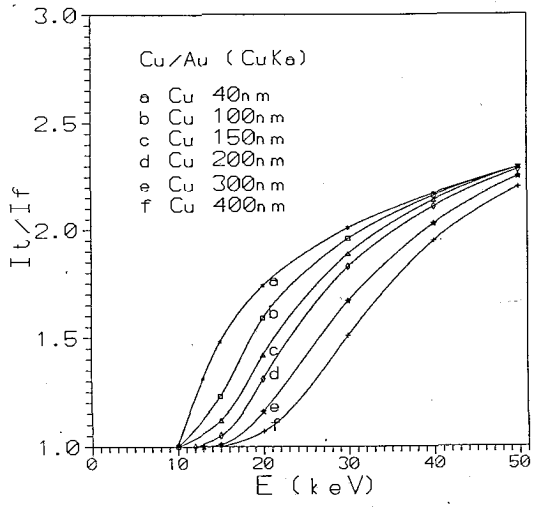

Fig. 1: Variation of the total X-ray signal I_t from an overlayer of Cu on a gold substrate normalised to the signal I_f from a thin unsupported film of the same thickness as a function of energy, for different overlayer thicknesses.

Experiments were also performed in order to verify the Monte-Carlo results.

Fig. 2 shows a series of experiments in comparison to our calculated results from reference [14]. The total normalised signal I_t/I_f is given. Al films, 40nm thick, on

various substrates are used. The agreement between calculations and experimental results is quite good in all cases within the limits of experimental and calculation errors.

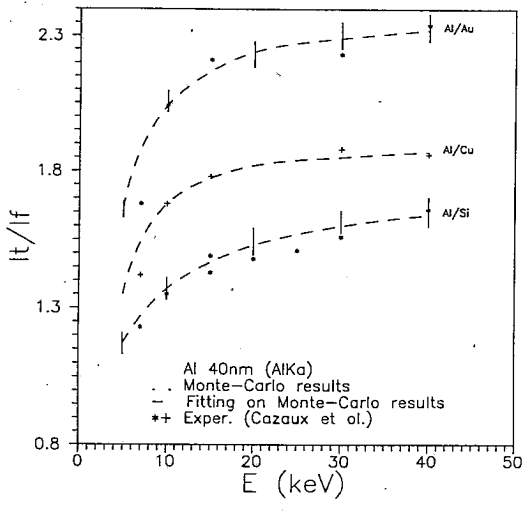

Fig. 2: A series of experiments in comparison to our calculated results. The total normalised signal I_t/I_f is given. Al films, 40nm thick, on various substrates are used.

The extent of the total x-ray signal in an x-y axis is calculated by the following way: A line is considered, which is defined by the intersection of the plane defined by the sample surface and that defined by the perpendicular to this surface and the direction of the incident beam (see fig. 3). The lateral extent of the x-ray signal is greater in this direction than in a direction perpendicular to that one. So the more restrictive case was considered. We then consider planes perpendicular to the above line and the calculated signal at each point of these planes in the interaction volume is attributed to one point of this line.

Fig. 4 shows the distribution of the total X-ray signal as defined above, for the case of a Cu film on Au (analysed line: CuKa). The film thickness was 40nm and

3 different angles of incidence were considered (30^0 (a), 60^0 (b) and 85^0 (c)) for different primary beam energies. When $\Theta=30^0$ and below and for high primary beam energies, the obtained distribution is quite similar to that of normal incidence (normally distributed around the point of incidence). The main contribution is that due to the primary beam and the other contributions constitute a low background, distributed over a very large area. At higher angles the extent of the signal is larger and it is several hundreds of nm at 85^0, being even larger at higher primary beam energies. When the film thickness is increased, the extent of the X-ray signal is increased and it is larger even at small angles of incidence (30^0) (see figs. 4a, b, c).

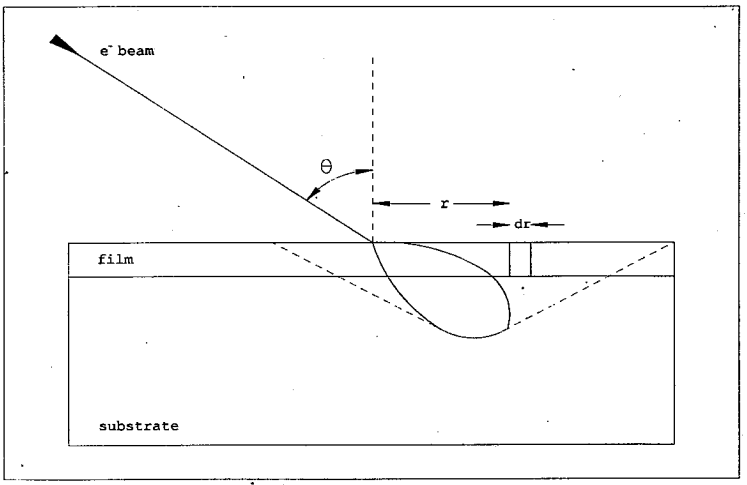

Fig. 3: The extent of the total X-ray signal is considered by projecting the calculated 3-D signal to a line defined by the plane of incidence and the sample surface.

From the obtained curves we can roughly estimate the resolving power of the technique at the corresponding conditions by considering the obtained distributions as "distorted gaussians" and applying the known criteria [18, 19].

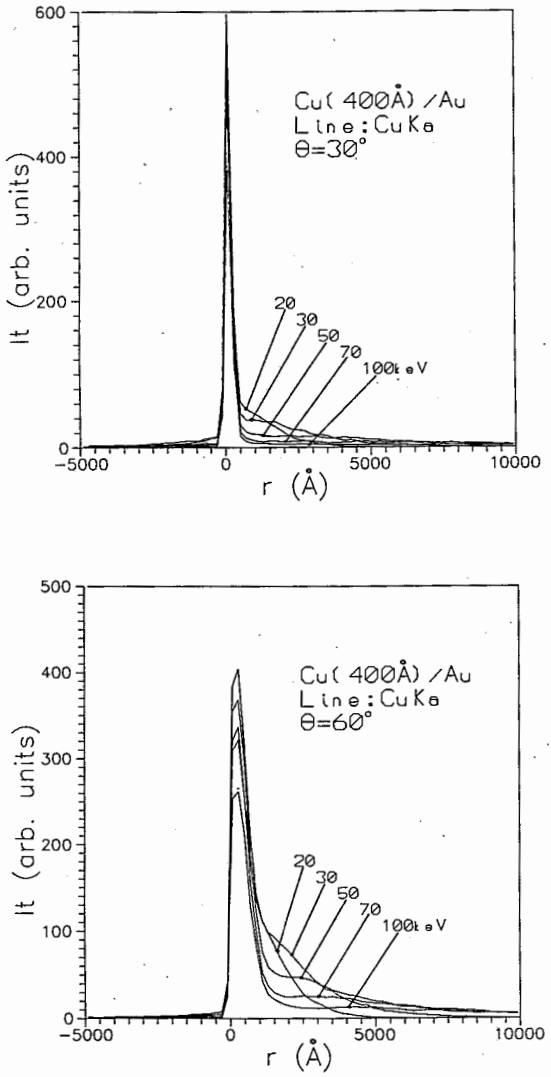

Fig. 4 (a, b): Radial distribution of the total X-ray signal for the case of a Cu film on Au (analysed line: CuKa). The film thickness was 40nm and 2 different angles of incidence were considered (30^0 (a), 60^0 (b)) for different primary beam energies.

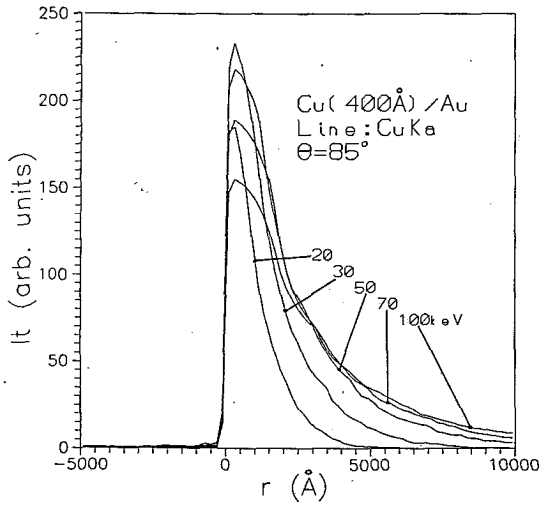

Fig. 4 (c): Radial distribution of the total X-ray signal for the case of a Cu film on Au (analysed line: CuKa). The film thickness and the angle of incidence was 40nm and 85^0 respectively (for different primary beam energies).

CONCLUSION

A Monte-Carlo programme has been developed for the determination of the X-ray signal from coatings, which takes into account all contributions to the total X-ray signal: a) signal induced by incident electrons b) backscattering from both the film and the substrate c) fluorescence due to characteristic X-rays and c) fluorescence due to continuous X-rays from the substrate. This programme may be used both for thin and for thicker coatings. It was applied to the case of a Copper film on Gold for different film thicknesses, primary beam energies and angles of incidence. The distribution of the X-ray signal in the projection of the plane of incidence on the sample surface is also calculated, with such parameters as the film thickness, the angle of incidence and the primary beam energy. The developed Monte-Carlo programme may be used both for the analysis of coatings and in the case of known composition for film thickness determination.

ΜΙΚΡΟΑΝΑΛΥΣΗ ΛΕΠΤΩΝ ΥΜΕΝΙΩΝ

Εφαρμόσαμε υπολογισμούς Monte-Carlo και πειραματικές μετρήσεις για μικροανάλυση ακτίνων Χ λεπτών υμενίων σε στερεό υπόστρωμα. Εξετάστηκαν τόσο το σήμα των ακτίνων Χ από το υμένιο όσο και η διακριτική ικανότητα της μεθόδου σαν συνάρτηση του πάχους του υμενίου, της ενέργειας και της γωνίας εισόδου της προσπίπτουσας ηλεκτρονικής δέσμης. Λάβαμε υπ' όψη όλες τις συνεισφορές στο μετρούμενο ολικό σήμα των ακτίνων Χ. Αυτές είναι:

α) Το επαγόμενο σήμα από την προσπίπτουσα ηλεκτρονική δέσμη.

β) Το επαγώμενο σήμα από οπισθοσκέδαση τόσο εντός του υμενίου όσο και εντός του υποστρώματος.

γ) Το επαγώμενο σήμα από συνεχή και χαρακτηριστική ακτινοβολία Χ, οι οποίες παράγονται στο υπόστρωμα από τα εισερχόμενα και οπισθοσκεδαζόμενα ηλεκτρόνια και ιονίζουν τα άτομα του υμενίου κατά την διαδρομή τους εντός αυτού.

REFERENCES

[1] R. Castaing and J. Descamps, Le Journal de Physique et le Radium, 16, 1955, 304.

[2] S. J. B. Reed, J. Appl. Phys., 16, 1965, 913.

[3] J. Philibert, Metaux, 465, 1964, 157.

[4] K. F. J. Heinrich, Adv. in X-ray Analysis, 11, 1968, 40.

[5] J. Philibert and D. Penot, Optique des rayons X et Microanalyse, ed. Hermann, Paris 1966, 365.

[6] W. Reuter, Proc. 6th Int. Conf. X-ray Opt. Micr., Univ. Tokyo Press 1972, 121.

[7] J. D. Brown, Spectrochimica Acta, 38B, 1983, 121.

[8] H. E. Bishop and D. M. Poole, J. Phys. D: Appl. Phys., 6, 1973, 1142.

[9] D. F. Kyser and K. Murata, Special Public., 460, 1976, 129.

[10] J. Foulu and J. Henoc, J. Microsc. Spectr. Electr., 2, 1977, 129.

[11] J. L. Pouchou and F. Pichoir, La Recherche Aerospatiale, 3, 1984, 167.
[12] J. L. Pouchou and F. Pichoir, La Recherche Aerospatiale, 5, 1984, 349.
[13] J. L. Pouchou and F. Pichoir, Proc. XII Inter. Congr. Electr. Micr., 2, 1990, 194.
[14] J. Cazaux, O. Jbara, A. G. Nassiopoulos and E. Valamontes, Proceed. 12th ICXOM, 1989, 201.
[15] J. Cazaux, O. Jbara and X. Thomas, Surf. Interf. Anal., 15, 1990, 567.
[16] A. G. Nassiopoulos and E. Valamontes, Surf. Interf. Anal., 15, 1990, 405.
[17] A. G. Nassiopoulos and E. Valamontes, Microbeam Analysis, 1, 1990, 161.
[18] A. G. Nassiopoulos and E. Valamontes, Inst. Phys. Conf. Ser., 117(2), 1991, 75.
[19] E. Valamontes, A. G. Nassiopoulos and N. Glezos, Surf. Interf. Anal., 19, 1992, 419.

Chimika Chronika, New Series, 26, 29-38 (1997)

COMPARISON OF SXRF AND EPMA FOR THE ELEMENTAL CHARACTERISATION OF THIN COATINGS.

E. Valamontes

Institute of Microelectronics, NRCPS "Demokritos", P.O. Box 60228, 153 10 Aghia Paraskevi, Attiki, Greece.

(Received: October 2, 1996 In final form: November 12, 1996)

Back-foil Scanning X-ray Microfluorescence, developed in a Scanning Electron Microscope and applied for the analysis of very thin coatings is compared with Electron Probe X-ray Microanalysis (EPMA). Both experimental results and Monte-Carlo calculations are used in this respect. The signal to background ratio as a function of the primary electron beam energy and angle of incidence and for different film thicknesses is obtained for both techniques and a comparative study of sensitivity is made. Back-foil Scanning X-ray Microfluorescence (SXRF) used in optimised experimental conditions, is found to be more sensitive than EPMA, especially in the case of film thicknesses below ≈100nm. The resolving power of Back-foil SXRF is also calculated for the anode used by Monte-Carlo simulations.

KEY WORDS: EPMA, SXRF, Coatings.

INTRODUCTION

X-ray Fluorescence (XRF) and X-ray Microanalysis (EPMA) are two analytical techniques with quite different characteristics. EPMA uses electron excitation in an Electron Microscope while XRF uses an X-ray excitation source, which offers several advantages over the electron excitation: a) Relative detection limits of the order of 1 ppm compared to ≈1000 ppm by weight in Energy Dispersive EPMA, b) possibility of analysing insulators without depositing a conducting layer on the top of them, c) possibility of nondestructive analysis of beam sensitive biological samples. On the other hand, EPMA offers the advantage of a much better lateral resolution, in the μm range, which allows imaging of the analysed element of the sample.

Several attempts have been made to use the electron source of the electron microscope in order to obtain an x-ray source inside the microscope. Middleman and Geller [1] fixed an attachment with a 25μm thick molybdenum foil, used as

an X-ray source, generated by a 30keV electron beam. Similar attachments have been proposed by Linnemann and Reimer [2], Wendt [3,4] and Weiss [5], all of them considering their transmission X-ray sources far from the specimen to be analysed. Little different, but always with the X-ray source far from the specimen were the attachments proposed by Eckert (both reflection [6] and transmission [7,8]) and Pozsgai (transmission mode, but with the analysed specimen in a closed space, protected from unwanted X-rays [9]). Other works, dealing with analogous SEM attachments, are nicely described in a review article by Pozsgai [10].

A different approach have been made by Cazaux [11] and implemented first in a surface analysis instrument [12] and later in a Scanning Electron Microscope [13]. It consists of using the anode in thin film form (X-ray source) in close contact to the sample, also in thin film form. The X-rays are created within the anode and ionise the atoms of the sample on their way out. The corresponding SEM attachment [13] is illustrated in Fig. 1. Compared to all the other proposed solutions, this experimental arrangement offers the ultimate resolution, which is in the μm range when the anode is sufficiently thin (of the order of the electron range). In this paper, this last solution is used (Back-foil Scanning X-ray Microfluorescence) and the sensitivity of the technique for the analysis of very thin overlayers, where EPMA reaches its detection limits, is examined. Both experimental results and Monte-Carlo simulations are used in this respect. Direct comparison with EPMA is also made. The radial distribution of the obtained fluorescence signal is also calculated by Monte-Carlo simulations.

RESULTS AND DISCUSSION

A) Experimental Setup.

The experimental setup of fig. 1 was used for back-foil XRF. The anode was composed of a nickel foil, 5μm thick. The anode was chosen sufficiently thick in order to prevent primary beam electrons to reach the Ti film on the back side of the anode. On the other hand, a limited thickness is necessary in order to minimize self-absorption of the generated x-rays. Titanium films of different

thicknesses were deposited on one side by electron gun evaporation in high vacuum (10^{-8} Torr). A Si(Li) detector and the EDAX system for quantitative analysis was used for x-ray signal acquisition. The x-ray signal, integrated under the peak and the integrated background, also under the peak and in the same energy window, were used. Standard EPMA, using the same experimental conditions of beam current and electron beam focussing was applied to the same samples.

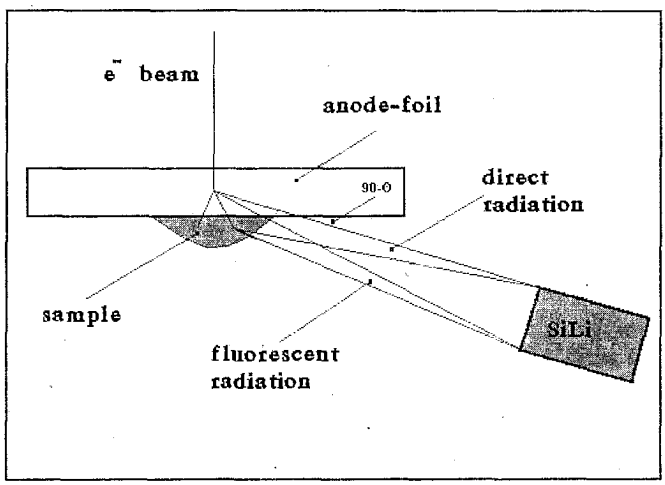

Fig. 1: Experimental setup used for back-foil XRF. Illustration of the trajectories of primary and fluorescence x-rays in back-foil XRF. The background is reduced by absorption of the continuous radiation, created by the electron beam, within the anode.

B) Monte-Carlo calculations.

The basic computational model for the calculation of electron trajectories was described in detail elsewhere [14]. It is based on the following assumptions:

- elastic scattering is described by screened Rutherford cross-section;
- angle deviation is considered to be due only to elastic scattering. This is a good approximation, as inelastic scattering occurs through very small angles;

- between two scattering points, electrons are considered to lose energy continuously. The energy loss is described by the Bethe equation for energies E>6.4J, where J is the mean ionisation potential. For lower energies, the Rao-Sahib and Wittry's expression is used.
- Each step length for elastic scattering is considered to be constant and equal to 1/100 of the total electron range (plural scattering model). The total length of the electron trajectory within the sample is taken to be the Bethe range. With this approximation, the calculation time is reduced significantly while little error is introduced. In order to evaluate the x-ray signal induced by electrons, each step is divided into smaller steps. At each small step, the energy and position of the electron is known, so the probability for x-ray generation is given by the corresponding cross section.

The x-ray emission is considered to be isotropic, two random numbers are used for the direction of x-ray emission. Part of them enter into the film after possible absorption within the anode.

The x-ray fluorescence signal is calculated by dividing the film in 10 layers and considering the probability that the primary x-rays entering the layer are absorbed by the layer on their way out of the film. Absorption correction of the fluorescent x-ray signal created within the film is also considered. The absorption coefficients used are taken from the x-ray cross-section compilation by the Kaman Science Corporation [16].

c) Results and Discussion.

Fig. 1 illustrates the trajectory of the direct and fluorescence x-rays in back-foil XRF. The background is reduced by absorption of the continuous radiation, created by the electron beam, within the anode.

Fig. 2 indicates the experimental results of the signal to background ratio (S/B) in the case of back-foil XRF for different film thicknesses as a function of the detection angle Θ. The acquisition time of the whole spectrum was equal to 600 sec. When this angle is increased, the S/B ratio is improved, due to further reduction of the background and an increase of the analysed film area.

Fig. 3 shows the ratio of the analysed Ti X-ray signal from the film to the Ni signal from the anode. Points correspond to experimental results and full lines to Monte-Carlo calculations. Good agreement is observed between experiment and

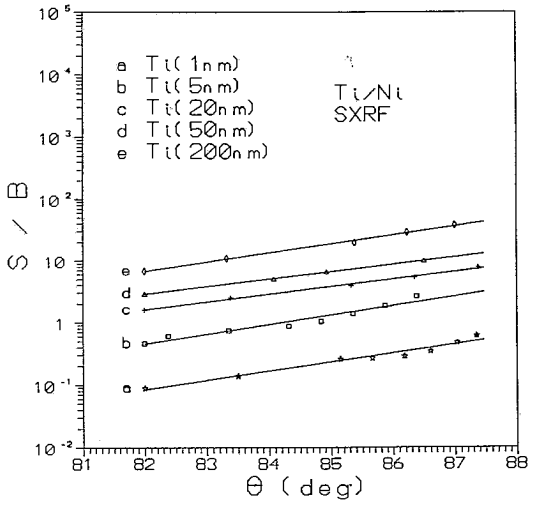

Fig. 2: Experimental values of the signal to background ratio (S/B) in the case of Back-foil XRF for different film thicknesses as a function of the detection angle Θ.

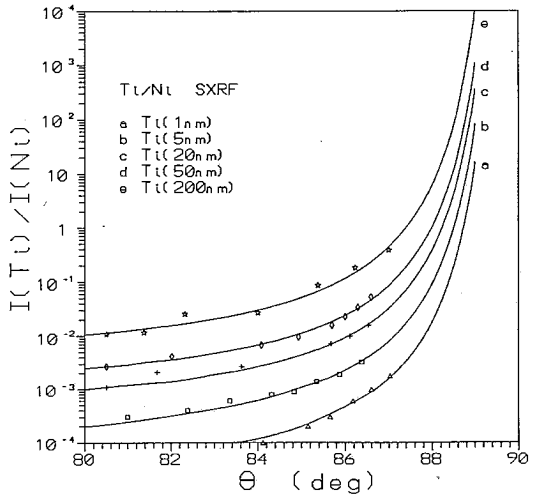

Fig. 3: Ratio of the Ti x-ray signal from the film to the Ni x-ray signal from the anode. Points correspond to experimental results and full lines to Monte-Carlo calculations.

calculations. The Ti signal from the film is increased with respect to the signal from the anode as the detection angle Θ is increased. This is due to an increase of the self-absorption of the Ni X-ray line and to an increased analysed area.

EPMA was performed on the same sample for comparison. The signal from a thin film in EPMA is improved at low primary beam energies and high angles of incidence. Figs. 4a, 4b and 4c illustrate experimental results of the signal to background ratio (S/B) for three different angles of incidence. If we compare fig. 2 with figs. 4a, 4b and 4c we see that in Back-foil XRF the signal to background ratio is 2 or 3 times higher than in EPMA. The same acquisition time was used for both EPMA and back-foil XRF spectra (600 sec). But it should be noted that the reduced background in the case of back-foil XRF permits to increase the acquisition time and improve sensitivity. Indeed the minimum detectable concetration (or thickness) is calculated by considering the Rose criterion, according to which a signal is detectable if the corresponding peak is at least 3 times the standard deviation of the background. By taking that into account the minimum detectable concentration X_m of an element A in a matrix may be expressed as:

$$X_m = \frac{3}{I_S} \cdot \sqrt{\frac{I_{BG}}{t}}$$

where I_S is the signal from a standard containing only element A and I_{BG} is the signal under the background. From the above expression it is obvious that the minimum detectable concentration is reduced if I_{BG} is smaller and the acquisition time is increased. In the case of back-foil XRF the reduced background gives the possibility to increase the measuring time so as the sensitivity of the technique is considerably improved compared to that of EPMA.

The lateral distribution of the total x-ray signal from the film in Back-foil XRF is given in fig. 5 for a primary beam energy of 30keV. This distribution is approximately gaussian with standard deviation σ_o=2.3μm. By applying the Rayleigh criterion as in reference [15], the resolving power of the technique, defined as the minimum distance between two points for which the x-ray signals are resolved, is calculated. A value of 3.7μm is found for the anode thickness

and primary beam energy used. This resolving power is by some orders of magnitude better than in standard XRF.

CONCLUSION

Back-foil XRF and EPMA are both applied to the analysis of very thin films. The sensitivity of Back-foil XRF is better than that of EPMA in the case of very small film thicknesses (some tens to some hundreds of $\overset{0}{A}$). The obtained experimental results are verified by Monte-Carlo calculations. The resolving power of Back-foil XRF is of the order of some microns. It is much better than in conventional XRF and of the same order of magnitude as in EPMA.

ΣΥΓΚΡΙΣΗ ΤΩΝ SXRF ΚΑΙ EPMA ΓΙΑ ΤΗΝ ΣΤΟΙΧΕΙΑΚΗ ΑΝΑΛΥΣΗ ΛΕΠΤΩΝ ΥΜΕΝΙΩΝ

Σε ηλεκτρονικό μικροσκόπιο σάρωσης αναπτύχθηκε μικροφθορισμός ακτίνων Χ με χρήση ανόδου (SXRF) και χρησιμοποιήθηκε για την ανάλυση πολύ λεπτών υμενίων συγκρινόμενος με την μικροανάλυση ακτίνων Χ ηλεκτρονικής δέσμης (EPMA). Στην κατεύθυνση αυτή χρησιμοποιήθηκαν τόσο πειραματικά αποτελέσματα όσο και υπολογισμοί Monte-Carlo. Υπολογίσθηκε ο λόγος σήμα προς υπόβαθρο σαν συνάρτηση της ενέργειας και της γωνίας εισόδου της προσπίπτουσας ηλεκτρονικής δέσμης και για διαφορετικά πάχη υμενίου. Ο μικροφθορισμός ακτίνων Χ με χρήση ανόδου (SXRF) βρέθηκε πιό ευαίσθητος από την μικροανάλυση ακτίνων Χ ηλεκτρονικής δέσμης (EPMA), ιδιαίτερα στη περίπτωση παχών υμενίου μικρότερων από 100nm. Ακόμη υπολογίσθηκε η διακριτική ικανότητα του μικροφθορισμού ακτίνων Χ με χρήση ανόδου (SXRF) με τη χρήση προσομοίωσης Monte-Carlo.

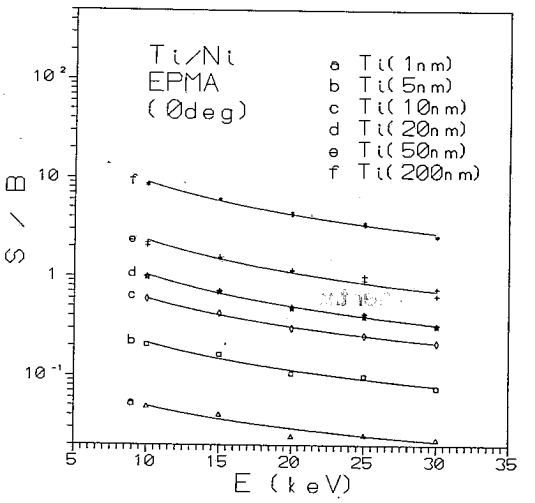

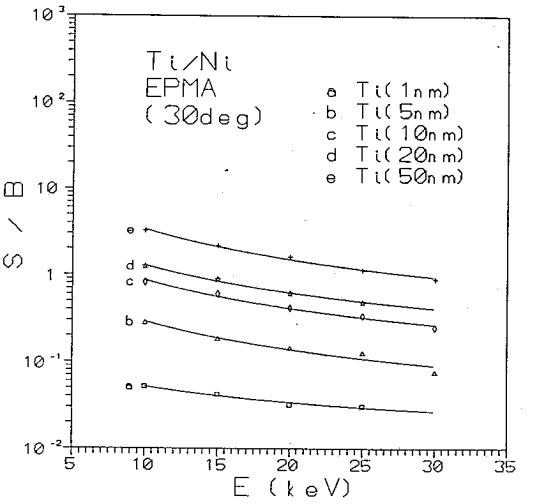

Fig 4 (a, b): Experimental values (EPMA) of the Signal to Background ratio (S/B) for two different angles of incidence (0, 30 deg).

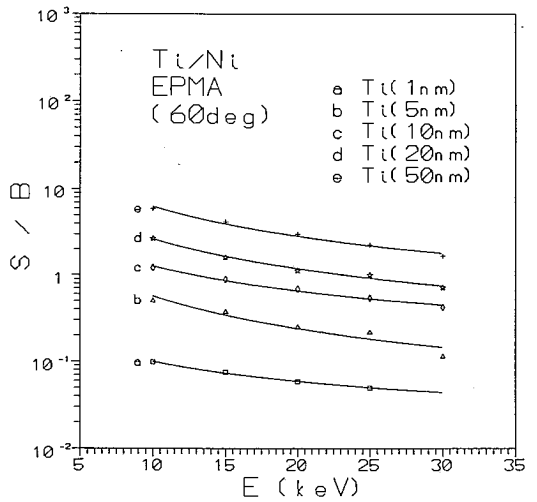

Fig 4 (c): Experimental values (EPMA) of the Signal to Background ratio (S/B) for 60 deg angle of incidence.

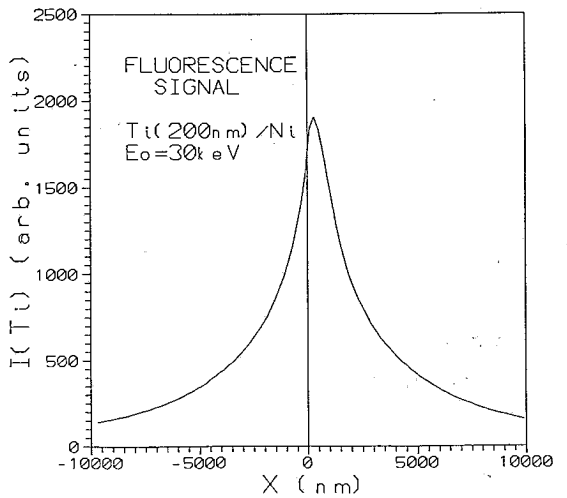

Fig 5: The lateral distribution of the total x-ray signal from a Ti(200nm) film in back-foil XRF for a primary beam energy of 30keV.

REFERENCES

[1] L. M. Middleman and J. D. Geller, Scanning Electron Microscopy, Part I, pp. 171-177, IITRI, Chicago 1976.

[2] B. Linnemann and L. Reimer, Scanning 1, 1978, 109.

[3] M. Wendt, Patentscrift DD-WP139, 304 1978.

[4] M. Wendt and Th. Krajewski in: Proc. of 5 Tagung Microsonde, Phisikalische der DDR, Leipzig, pp. 125-129, 1981.

[5] R. M. Weiss, Beitn. Elektronmikroskop. Direktabl. Oberfl., 12, 209, 1979.

[6] R. Eckert in: Scanning Electron Microscopy, Vol. IV, pp. 1535-1545, SEM inc, AMF O' Hare (Chicago) 1983.

[7] W. Plannet, Leaflet Rontgenbox, Plano Marburg, Germany 1983.

[8] R. Eckert, Scanning 8, 232, 1986.

[9] I. Pozsgai, Inst. Phys. Conf. Ser. No 78, 201, 1985.

[10] I. Pozsgai, X-ray Spectrometry, Vol. 20, 215-223, 1991.

[11] J. Cazaux, Rev. Phys. Appl. 10, 263, 1975.

[12] D. Mouze, X. Thomas and J. Cazaux in: Proceed. of 11th Internat. Congr. on X-ray Optics and Microanalysis, edited by: J. D. Brown and R. H. Packwood, pp. 63-66, London, Canada 1986.

[13] E. Valamontes and A. G. Nassiopoulos in: Proceedings of III Balkan Congress on Electron Microscopy, Athens, pp. 267-268, 1989.

[14] A. G. Nassiopoulos and E. Valamontes, Surf. Interf. Anal., 15, 1990, 405.

[15] E. Valamontes, A. G. Nassiopoulos and N. Glezos, Surf. Interf. Anal., 19, 1992, 419.

[16] X-ray Cross-section Compilations from 0.1 keV to 1 MeV. Kaman Science Corporation, Colorado Springs, Colorado 80907.

Chimika Chronika, New Series, 26, 39-48 (1997)

Reduction of aromatic nitrocompounds on carbon fibre electrodes in propylene carbonate solutions

A.Pelekourtsa-N.Missaelidis-D.Jannakoudakis
Laboratory of Physical Chemistry, University of Thessaloniki
54006 Thessaloniki-Greece

(Received: May 8, 1996 In final form: December 9, 1996)

Abstract

The electrochemical behavior of aromatic nitrocompounds in propylene carbonate solutions in the absence and in the presence of a proton donor, as well as the influence of the Li^+-cations on the reduction of these depolarizers are investigated on carbon fibre electrodes.

In the case of nitrobenzene, two reduction steps appear; the first corresponds to the formation of the radical anion and the second to the further reduction to phenyl-hydroxylamine. In the case of dinitrobenzenes, a dianion diradical is formed in two successive and reversible one electron steps; the dianion is only partially further reduced at higher negative potentials. The dianion of p-dinitrobenzene remains stable over a large potential range, due to its quinonoid structure.

With the introduction of Li^+ in the PC solutions of the nitrocompounds a significant shift of the reduction waves to more positive potentials was observed, due to the formation of ion pairs between the radical anions and the Li^+-cations.

In the presence of benzoic acid as a proton-donor, the reduction of nitrobenzene occurs directly to phenylhydroxylamine. Also in the presence of a proton-donor p- and o-dinitrobenzene are reduced first to nitrophenylhydroxylamine and then to phenylenediamine, while m-dinitro-benzene is reduced first to m-nitrophenylhydroxylamine and subsequently to m-phenyl-hydroxylamine. A similar result is achieved by the carboxylic groups which are formed on the carbon surface by the thermal and electrochemical oxidation of the carbon fibres.

Key words: Cyclovoltammetry, Nitrocompounds, Carbon Fibres, Propylene Carbonate

Introduction

Recently, in the electrochemical technology of non aqueous solutions, the use of the carbonic acid ester with propyleneglycole-1,2, the well known propylene carbonate (PC) is widely increased.

This aprotic solvent has a significant dissolving ability for several salts and many organic compounds, which can be used as depolarizers in the field of Electrochemistry. It has no corrosive properties, it is very stable in a large temperature range, it causes a remarkable ionisation to the dissolved salts, because of its high dielectric constant (ε=65) and furthermore cannot be oxidised or reduced within the commonly used potential range in the electrochemical technology. So, the propylene carbonate solvent with the proper salts can be used as a very good "supporting electrolyte system" in specific electrolytical reductions as well as oxidations and electrosynthesis in general, also in galvanic cells, when non-aqueous solvents are required (such as Li cells). On the other hand, in the electrochemical processes and electro-oxido-reductions, proper electrodes are the carbon fibres [1]. Very good electrochemical results occur when carbon fibre electrodes, obtained by graphitisation of polyacrylonitrile (PAN-based carbon fibres) are used [2-11].

The electro-reduction of aromatic nitrocompounds is very important in the field of electrosynthesis; these nitrocompounds can also be used as depolarizers in galvanic cells. The nitrocompound is, in general, one of the best "electrophores" [1].

The electro-reduction of aromatic nitrocompounds on carbon fibre electrodes in propylene carbonate solutions does not have any references in the international literature. For this reason we tried to investigate the above reduction by means of cyclic voltammetry.

Experimental

The solvent propylene carbonate has been purified by percolation through molecular sieves followed by distillation under vacuum.
Depolarizers: nitrobenzene, o,-m-,p-dinitrobenzene.
Supporting electrolytes: tetraethylammoniumperchlorate and lithiumperchlorate.
Proton donor: benzoic acid.
Electrodes: a)pristine carbon fibres, b)activated (modified) carbon fibres by thermal and electrochemical oxidation.

Bundles of highly oriented and mechanically stable PAN-based carbon fibres (Celion GY-70, BASF specific resistance 7×10^{-4} Ω·cm) were treated before use with MeOH and ultrasonic vibration. The electrochemically active surface of the carbon fibres has been estimated equal to 1,7 $cm^2 \cdot mg^{-1}$. The thermal oxidation of the fibres was carried out in the presence of air and water vapour at 160°C for 10h. The electrochemical oxidation was achieved by the controlled potential double-pulse oxidation in 0,5 M Na_2SO_4 for 6min. The thermal pre-treatment leads to the formation of carboxylic groups on the surface of the fibres, while the electrochemical oxidation causes the formation of oxygen containing functional groups which are also situated in the bulk of the fibres [12,13].

Cyclic voltammetry was carried out using a conventional set-up. The current densities are expressed per mg of fibres. The reference electrode was Ag/AgCl in PC and the potential values were expressed in reference to the hydrogen electrode. All experimental data are given at the temperature of 25°C.

Results and discussion

The cyclovoltammetric study of nitrobenzene on pristine carbon fibre electrodes in PC solutions proved that in the absence of a proton donor the reduction occurs in two well formed steps (Fig.1).

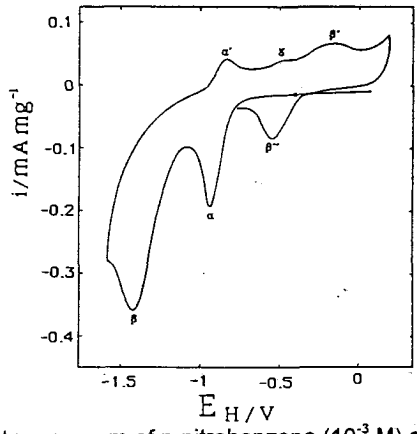

Fig. 1. Cyclic voltammogram of p-nitrobenzene (10^{-3} M) on pristine carbon fibres electrode in PC solution (Et_4NClO_4 0,1 M), v=100 $mVsec^{-1}$.

The reversible step (α) corresponds to the formation of the radical anion, which is further irreversibly reduced to phenylhydroxylamine (β) at higher negative potentials. The couple of peaks β′-β″ corresponds to the system nitrosobenzene-phenylhydroxylamine and peak γ to the oxidation of an intermediate reduction product formed because of the aprotic character of the solvent [14].

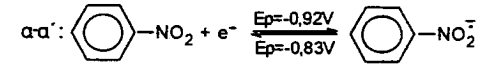

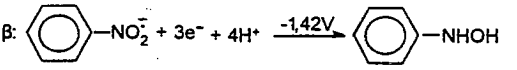

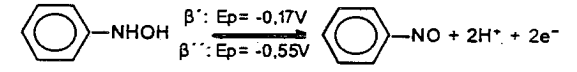

The electro-reduction of the aromatic nitrocompounds is substantially facilitated in the presence of a suitable proton donor, such as benzoic acid. This acid is not ionised in PC, as the conductometric study has shown; moreover it has a similar diffusion coefficient such as those of the aromatic nitrocompounds. For these reasons benzoic acid acts as a real proton donor during the electro-reduction of the aromatic nitrocompounds in the interfacial region.

In presence of benzoic acid, in fourfold quantity with respect to that of the depolarizer, nitrobenzene is reduced in one 4-electron step (Fig.2, peak α). In this case the couple of peaks α′-α″ corresponding to the redox-system nitrosobenzene-phenylhydroxylamine appears more reversible.

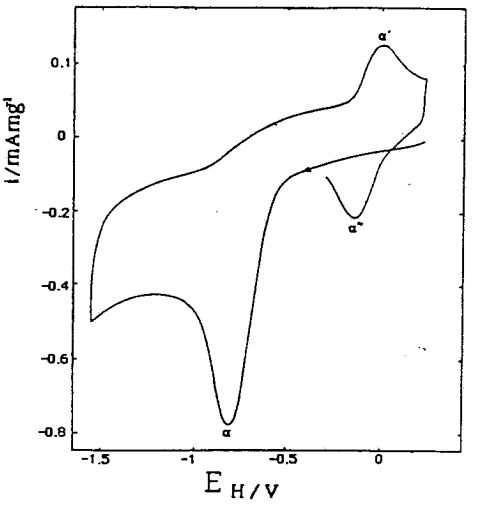

Fig. 2. Cyclic voltammogram of nitrobenzene (10^{-3} M) on pristine carbon fibres electrode in PC solution (Et_4NClO_4 0,1 M) in presence of benzoic acid ($4 \cdot 10^{-3}$ M), v=100 $mVsec^{-1}$.

The electro-reduction of the isomeric dinitrobenzenes on carbon fibre electrodes in PC solutions in the absence and in the presence of a proton-donor is furthermore studied.

In the absence of a proton donor a dianion diradical is formed in two successive reversible one-electron steps. In the case of p-dinitrobenzene the corresponding dianion remains stable within a large potential range (Fig. 3), due to its thermodynamically stable quinonoid structure and so it is only partially further reduced at a higher negative potential value to p-phenylenediamine.

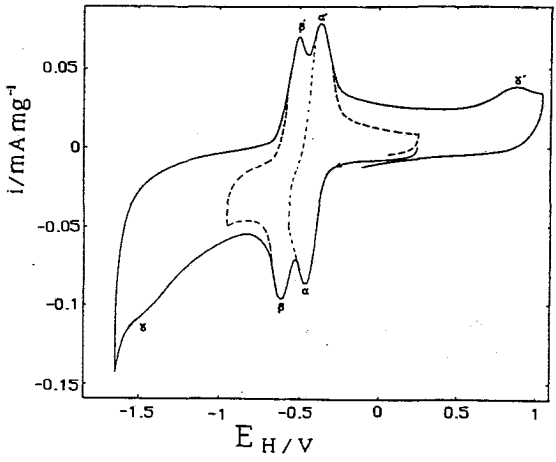

Fig. 3. Cyclic voltammogram of p-dinitrobenzene ($5 \cdot 10^{-4}$ M) on pristine carbon fibres electrode in PC solution (Et_4NClO_4 0,05 M), v=100 mVsec^{-1}.

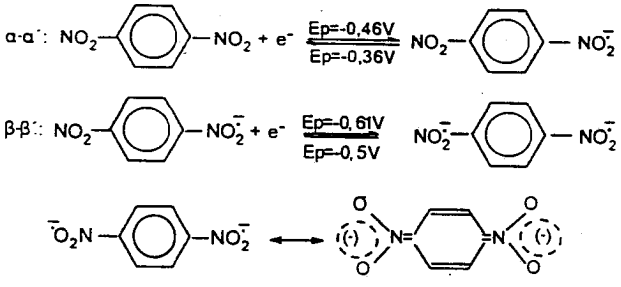

In the case of o-dinitrobenzene the diradical dianion cannot be stabilized taking the quinonoide structure because of stereochemical effects

dianion of o-dinitrobenzene

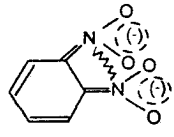

and so it is further reduced to o-phenylenediamine at more positive potential values than the diradical dianion of p-dinitrobenzene.

m-dinitrobenzene cannot take the quinonoid structure because of the meta-position of the substituents and so the further reduction of the corresponding diradical dianion to the final reduction product occurs at slightly more positive potential values than the dianion diradical of p-nitrobenzene.

In the presence of suitable quantities of benzoic acid as a proton donor the reduction of the dinitrobenzenes in PC solutions is completed in two steps.

Below are given the cyclic voltammogram of p-dinitrobenzene in presence of a twelvefold quantity of benzoic acid (Fig. 4) and the according reactions.

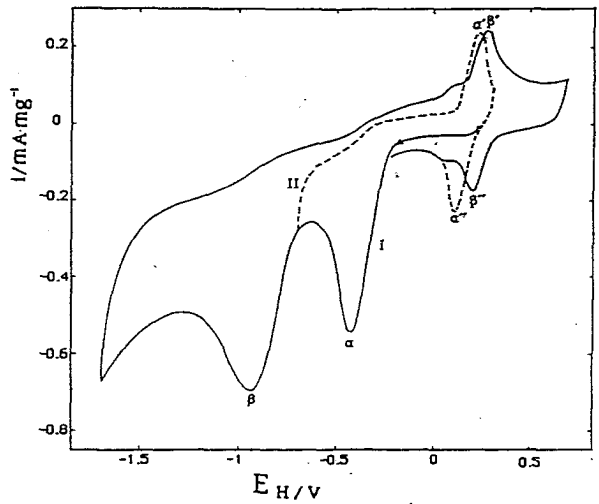

Fig. 4. Cyclic voltammogram of p-dinitrobenzene ($5 \cdot 10^{-4}$ M) on pristine carbon fibres electrode in PC solution (Et_4NClO_4 0,1 M) in presence of benzoic acid ($12 \times 5 \cdot 10^{-4} = 6 \cdot 10^{-3}$ M), v=100 mVsec^{-1}.

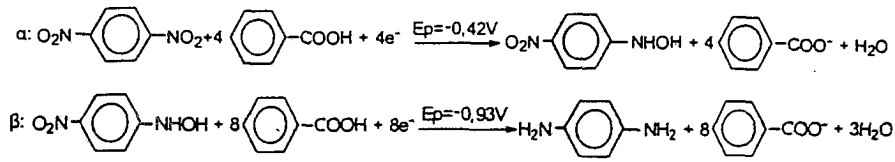

Peak α corresponds to the reduction of p-dinitrobenzene to p-nitrophenylhydroxylamine and peak β to its further reduction to p-phenylenediamine (a total of a 12-electron capture). The couple of peaks α′,α″ corresponds to the p-nitrophenylhydroxylamine-oxidation to p-nitroso-nitrobenzene and its rereduction to p-nitrophenylhydroxylamine. The couple of peaks β′,β″ corresponds to the p-phenylenediamine-oxidation to p-phenylenediimine and its rereduction to p-phenylenediamine.

The behavior of o-dinitrobenzene in the presence of a twelvefold quantity of benzoic acid is similar to that of p-dinitrobenzene. So the reduction of p-dinitrobenzene occurs in one 4-electron step to o-nitrophenylhydroxylamine and one 8-electron step to o-phenylenediamine (a total of a 12-electron capture).

On the contrary, m-dinitrobenzene is first reduced to m-nitrophenylhydroxylamine, but its further reduction leads to m-phenylenedihydroxylamine (a total of an 8-electron capture). So the whole reduction wave can be well formed in the presence of an eightfold quantity of benzoic acid. The corresponding cyclic voltammogram (Fig. 5) and the according reactions are shown below.

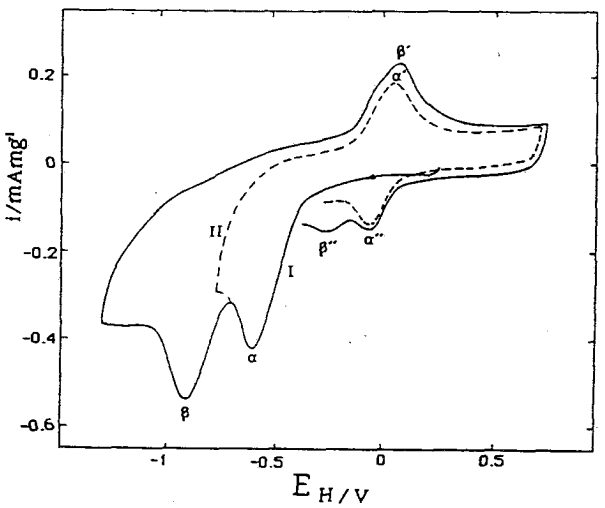

Fig. 5. Cyclic voltammogram of m-dinitrobenzene ($5 \cdot 10^{-4}$ M) on pristine carbon fibres electrode in PC solution (Et_4NClO_4 0,1 M) in presence of benzoic acid ($8 \times 5 \cdot 10^{-4} = 4 \cdot 10^{-3}$ M), v=100 mVsec^{-1}.

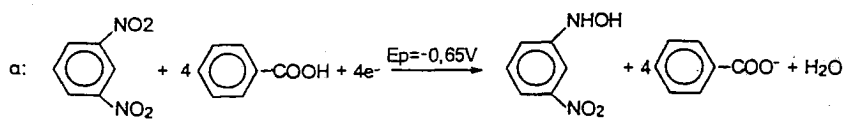

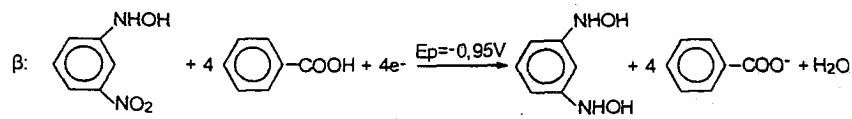

The couple of peaks α',α'' corresponds to the oxidation of m-nitrophenylhydroxylamine to m-nitrosonitrobenzene and its rereduction to m-nitrophenylhydroxylamine. The peak β' consists in reality of two not clearly defined steps corresponding to the oxidation of m-phenylenedihydroxylamine to m-dinitrosobenzene, which is further reduced to m-phenylenedihydroxylamine in two well defined steps α'',β''.

A similar catalytic effect also appears by the carboxylic groups which are formed on the carbon fibres by thermal and electrochemical oxidation. As an example cyclic voltammograms of nitrobenzene on thermal oxidised carbon fibres (Fig. 6) and on pristine carbon fibres in the presence of benzoic acid (Fig. 7) are given below.

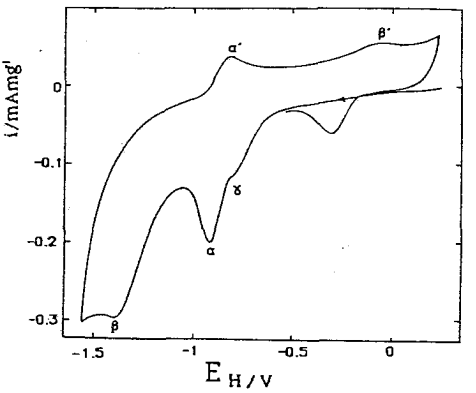

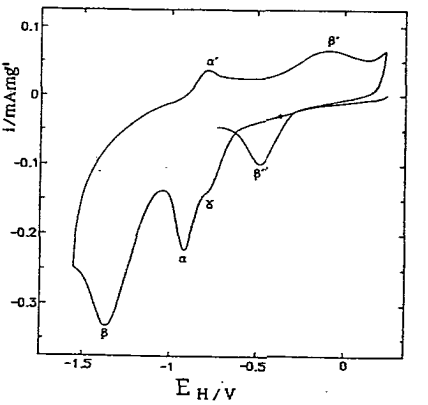

Fig. 6. **Fig. 7.**

Cyclic voltammograms of nitrobenzene (10^{-3} M) in PC solution (Et_4NClO_4 0,1 M), v=100 $mVsec^{-1}$

Fig. 6. on thermal oxidised carbon fibres (the thermal oxidation was carried out in the presence of air and water vapour at 160°C for 10 hours).

Fig. 7. on pristine carbon fibres in the presence of isomolecular quantity of benzoic acid (10^{-3} M).

Concluding from the comparison of the above cyclic voltammograms it is obvious that the carboxylic groups which are formed on the carbon fibres by thermal oxidation are enough to cause a catalytic effect on the electro-reduction of 10^{-3} M nitrobenzene, which is similar to that of an isomolecular benzoic acid quantity. The pre-wave γ corresponds to the reduction of 1/4 of the nitrobenzene quantity to phenylhydroxylamine. The rest of the nitrobenzene is reduced (to phenylhydroxylamine) in two steps α,β. By increasing the pre-treatment time the thermal oxidised fibres are able to catalyse the electro-reduction of the whole nitrobenzene quantity in one 4-electron step.

The electro-reduction of the aromatic nitrocompounds in PC solutions on carbon fibre electrodes is substantially facilitated in the presence of Li^+-cations . The introduction of $LiClO_4$ leads to the formation of ion pairs between the radical anions and the Li^+-cations.

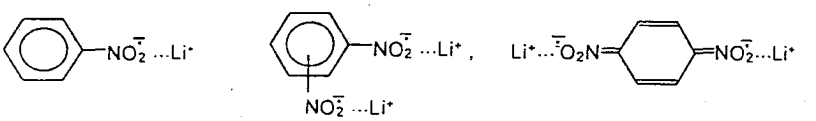

The ion pairs take the additional electrons during a succeeding fast heterogenous effect. This effect produces a significant shift of the reduction waves to more positive potential values.

In the case of nitrobenzene in the presence of Li^+-cations the reduction to phenylhydroxylamine occurs in one 4-electron step inspite of the aprotic character of the solvent (Fig. 8). In the case of p-dinitrobenzene the two one-electron steps are connected to one 2-electron step (α), which corresponds to the formation of the anion diradical, and the whole reduction wave is shifted towards more positive potential values (Fig. 9).

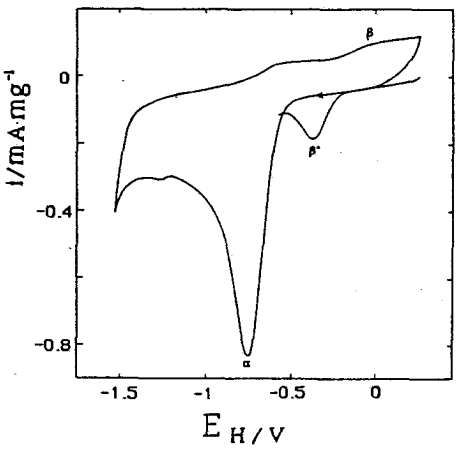

Fig. 8.

Fig. 8. Cyclic voltammogram of nitrobenzene (10^{-3} M) on pristine carbon fibres electrode in PC solution in presence of $LiClO_4$ 0,1 M, v=100 $mVsec^{-1}$.

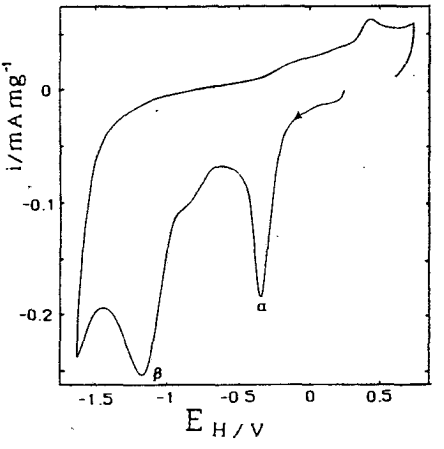

Fig. 9.

Fig. 9. Cyclic voltammogram of p-dinitrobenzene ($5 \cdot 10^{-4}$ M) on pristine carbon fibres electrode in PC solution in presence of $LiClO_4$ 0,05 M, v=100 $mVsec^{-1}$.

In general, Li^+-cations have a catalytic effect on the electro-reduction of these organic compounds, which are reduced over the intermediate formation of an anion radical.

Conclusion

The electro-reduction of the aromatic nitrocompounds in the solvent propylene carbonate on carbon fibre electrodes occurs over the intermediate formation of radical anions, which are reduced to the final product only at higher negative potentials because of the aprotic character of the solvent.

The above electro-reduction can be facilitated with the introduction of benzoic acid in molecular quantities, which are equivalent to the electron-number corresponding to the electro-reduction.

A similar result is obtained by the carboxylic groups, which are formed on the carbon surface by their thermal and electrochemical oxidation.

The Li^+-cations have a catalytic effect on the reduction of the aromatic nitrocompounds, due to the formation of ion-pairs between the radical anions and the Li^+-cations, which take the additional electrons during a succeeding fast heterogeneous process.

ΠΕΡΙΛΗΨΗ

Αναγωγή αρωματικών νιτροενώσεων σε ηλεκτρόδια ινών άνθρακα μέσα σε ανθρακικό προπυλενεστέρα.

Από την ηλεκτροχημική μελέτη του νιτροβενζολίου και των τριών ισομερών δινιτροβενζολίων (ο-, μ-, π-)μέσα στο διαλύτη propylene carbonate σε ηλεκτρόδια από αρχικές γραφιτικές ίνες προέκυψαν τα εξής:

Οι αρωματικές νιτροενώσεις απουσία δότη πρωτονίων ανάγονται σχηματίζοντας αρχικά ανιονικές ρίζες, οι οποίες λόγω του απρωτικού χαρακτήρα του PC ανάγονται προς το τελικό προϊόν σε αρνητικότερες τιμές δυναμικού.

Με την προσθήκη δότη πρωτονίων και συγκεκριμένα του βενζοϊκού οξέος στα διαλύματα του νιτροβενζολίου και των ισομερών δινιτροβενζολίων διευκολύνεται γενικά πολύ η αναγωγή των ενώσεων αυτών.

Έτσι το νιτροβενζόλιο με τετραμοριακή ποσότητα βενζοϊκού οξέος ανάγεται σε μια βαθμίδα προς φαινυλυδροξυλαμίνη. Το ο- και το π-δινιτροβενζόλιο με δωδεκαμοριακή ποσότητα βενζοϊκού οξέος ανάγονται σε δύο βαθμίδες πρώτα προς την αντίστοιχη νιτροφαινυλυδροξυλαμίνη και ύστερα προς την αντίστοιχη φαινυλενοδιαμίνη, ενώ το μ-ισομερές με οκταμοριακή ποσότητα βενζοϊκού οξέος ανάγεται σε δυο βαθμίδες προς μ-φαινυλενοδιυδροξυλαμίνη.

Η ηλεκτροαναγωγή των νιτροενώσεων διευκολύνεται επίσης από γραφιτικές ίνες στις οποίες ύστερα από θερμική ή ηλεκτροχημική οξείδωση δημιουργούνται καρβοξυλικές ομάδες, οι οποίες δρουν ως δότες πρωτονίων, οπότε η ηλεκτροαναγωγή των νιτροενώσεων γίνεται με παρόμοιο τρόπο όπως με την παρουσία του βενζοϊκού οξέος.

Με την προσθήκη $LiClO_4$ στο διάλυμα των νιτροενώσεων τα ιόντα του λιθίου σχηματίζουν ζεύγη ιόντων με τις ανιονικές ρίζες τους. Τα ζεύγη αυτά λόγω μικρής διαλυτότητας στο PC επικάθονται στην επιφάνεια των ηλεκτροδίων του άνθρακα και προσλαμβάνουν ευκολότερα τα υπόλοιπα ηλεκτρόνια που απαιτούνται για την περαιτέρω αναγωγή. Έτσι με την προσθήκη $LiClO_4$ το μεν νιτροβενζόλιο ανάγεται σε μια μόνο τετραηλεκτρονική βαθμίδα προς φαινυλυδροξυλαμίνη, ενώ στο π-δινιτροβενζόλιο οι δύο μονοηλεκτρονικές βαθμίδες ενώνονται σε μια βαθμίδα και συγχρόνως όλο το κύμα αναγωγής μετατοπίζεται σε θετικότερες τιμές δυναμικού.

LITERATURE

1. D. Kyriacou, D. Jannakoudakis, Electrocatalysis of Organic Synthesis, John Wiley and Sons, N.Y. 1986, p.35.
2. E. Theodoridou and D. Jannakoudakis, Z. Naturforsch. 36b. (1981) 840.
3. E. Theodoridou, P. Karabinas and D. Jannakoudakis, Z. Naturforsch. 37b. (1982) 97.
4. A.D. Jannakoudakis, E. Theodoridou, Z. Phys. Chem. N.F. 129 (1982) 197.
5. P.D. Jannakoudakis and E. Theodoridou, Z. Phys. Chem. N.F. 130 (1982) 49.
6. P.D. Jannakoudakis and E. Theodoridou, Z. Phys. Chem. N.F. 130 (1982) 167.
7. E. Theodoridou, A.D. Jannakoudakis, Z. Phys. Chem. N.F. 132 (1982) 175.
8. E. Theodoridou, A.D. Jannakoudakis and D. Jannakoudakis, Z. Phys. Chem. N.F. 134 (1983) 227.
8. N. Missaelidis, E. Theodoridou and D. Jannakoudakis, Chim. Chron. N.S. 13 (1984) 45.
10. A.D. Jannakoudakis, C. Tsiamis, P.D. Jannakoudakis, E. Theodoridou, J. Electroanal. Chem. 184 (1985) 123.
11. D. Kyriacou, D. Jannakoudakis, Electrocatalysis for Organic Synthesis, John Wiley and Sons N.Y. 1986, p.69.
12. B.F. Watkins, J.R. Behling, E. Kariyand, L.L. Miller, J. Am. Chem. Soc. 97 (1975) 3549.
13. A.D. Jannakoudakis, P.D. Jannakoudakis, E. Theodoridou, J.O. Besenhard, Journal of Applied Electrochemistry 20 (1990) 619.
14. L. Holleck und D. Becher, J. Electroanal. Chem. 4 (1962) 321.

Chimika Chronika, New Series, 26, 49-56 (1997)

Cyclovoltammetric study of the system p-benzoquinone-p-hydroquinone on carbon-fibre, platinum and platinized carbon fibre electrodes in propylene carbonate solutions

A.Pelekourtsa, N.Missaelidis, D.Jannakoudakis
Laboratory of Physical Chemistry, University of Thessaloniki
54006 Thessaloniki-Greece

(Received: May 8, 1996 In final form: December 9, 1996)

Abstract

The electrochemical behavior of the redox system p-benzoquinone - p-hydroquinone on carbon fibre electrodes is investigated in propylene carbonate (PC) solutions by the cyclic voltammetric method.

It is established that, in the absence of a proton donor the reduction, as well as the oxidation, takes place in two separate one-electron steps. However, in the presence of a bimolecular quantity of proton donor both, the reduction and oxidation, occur absolutely reversibly in one bielectronic step. The electrochemical characteristics of the reversible bielectronic step allow a perfect estimation of the electrochemically active surface of electrodes in PC. For this reason, the above procedure is proposed as determination-method of the electrochemically active surface of solid electrodes in PC since the well known system $Fe(CN)_6^{3-}$ - $Fe(CN)_6^{4-}$ cannot be employed in these solutions, because the ferrocyanide salts have a small solubility in PC.

Key words: Cyclovoltammetry, Benzoquinone, Carbon Fibres, Propylene Carbonate

Introduction

Propylene carbonate (PC) is the ester of carbonic acid with propyleneglycol-1,2. The interest for this solvent has recently been greatly increased, because it is widely used in non-aqueous galvanic cells (like Li batteries) and in the non-aqueous-solution- Electrochemistry in general.

The electrochemical cells in non-aqueous solutions were invented so that we can take advantage of the alkalimetals' and alkali-earth metals' high potential and a proper solvent for these cells is the aprotic solvent propylene carbonate. PC is stable in a large temperature range, it has no corrosive properties, it can dissolve and ionise many salts and it is easily prepared and simply purified. The physicochemical constants of PC at the temperature of 25°C are the following: dielectric constant ε=65, refraction index n=1,42, density d=1,2 gr/cm^3, viscosity coefficient n=2,5 cp, dipole moment μ=5,2 Debye [1,2]. Moreover, the main advantage of PC is that it cannot be oxidised or reduced within the potential ranges which are frequently used in electrolytical systems and electrochemical cells. So, the propylene carbonate solvent with the proper salts can be used as a very good "supporting electrolyte system" in specific electrolytical reductions as well as oxidations and electrosynthesis in general, also in non aqueous galvanic cells (such as Li cells).

Propylene carbonate can be used for the study of several depolarizers on various electrodes. Very convenient electrodes for this purpose are the carbon fibres obtained by the graphitisation of polyacrylonitrile as well as the platinized carbon fibres prepared by electrodeposition of platinum on carbon fibres from solutions of its compounds. These electrodes have already been used in many studies in our laboratory, using other solvents than PC [3-14].

In the present study the electrochemical behavior of the p-benzoquinone oxidoreductive system on carbon-fibre, platinum and platinized carbon fibre electrodes is investigated, in order to find out how the above system behaves in PC. The use of p-benzoquinone for the estimation of the electrochemically active surface of solid electrodes is also of great importance, because the commonly used redox-system $Fe(CN)_6^{3-}$ - $Fe(CN)_6^{4-}$ is not convenient for PC solutions, as none of the usual ferrocyanide salts is soluble in PC.

Experimental

Solvent: Propylene carbonate (Fluka A.G. «purum»). PC has been purified by percolation through molecular sieves followed by distillation under vacuum.
Depolarizer: p-benzoquinone (Fluka A.G. «puriss p.a.»)
Supporting electrolyte: tetraethylammonium perchlorate (Fluka A.G. «purum»)
Proton-donor: benzoic acid (Merck «zur Analyse»)
Electrodes: a)pristine carbon fibres, b)bulk platinum globe, c)platinized carbon fibres.

Bundles of highly oriented and mechanically stable PAN-based carbon fibres (Celion GY-70, BASF; density 2 $g \cdot cm^{-3}$, Young's modulus 5×10^{11} $N \cdot m^{-2}$, specific resistance 7×10^{-4} $\Omega \cdot cm$) used in this study were treated before use with MeOH and ultrasonic vibration, rinsed with water and vacuum dried, in order to remove the adhesive resins which were deposited during the production process. Platinized carbon fibre electrodes have been prepared by simple electrodeposition of platinum on carbon fibres. This was performed by leaving the fibres at the potential at which hydrogen evolution also begins in acidic aqueous solutions of H_2PtCl_6 ($c=10^{-3}$ M) for 10min [14].

Cyclic voltammetry was carried out using a conventional set-up. The current densities are expressed per mg of fibres. The reference electrode was Ag/AgCl in PC and the potential values were expressed in reference to the hydrogen electrode. All experimental data are given at the temperature of 25°C.

Results and discussion

In Fig.(1) the form and the position of the cyclic voltammogram of p-benzoquinone on pristine carbon fibre electrodes in PC solution is given as an example. Observing this voltammogram it is obvious that p-benzoquinone is reduced in two well-defined one-electron steps (α) and (β), which correspond to the following reactions:

(I) 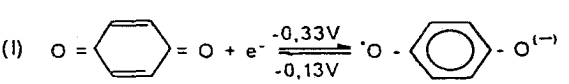

(II) 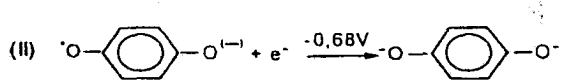

At the anodic part of the wave, there is a "break" (β′) corresponding to the irreversible reaction (II) and also a well-formed peak (α′) which, together with peak (α), represent the satisfactorily reversible reaction (I). The satisfactory reversibility of the reaction (I) is also proved by the appearance of the couple-peaks (α) and (α′) if the sweep is interrupted, after the first cathodic step.

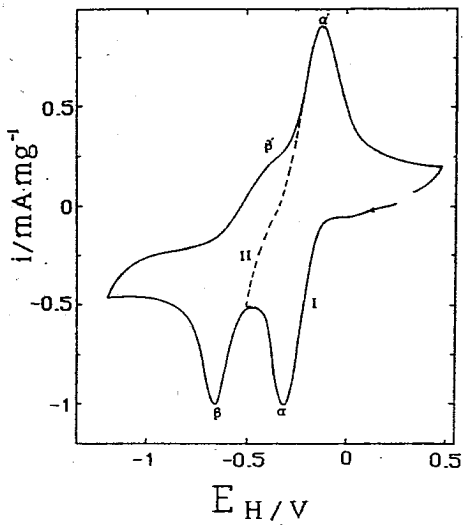

Fig. 1. Cyclic voltammogram of p-benzoquinone ($5 \cdot 10^{-3}$ M) on pristine carbon fibres electrode in PC solution (Et_4NClO_4 0,25 M), v=100 $mVsec^{-1}$.

The electroreduction of p-benzoquinone in PC is further studied on platinized carbon fibres and on bulk platinum electrodes. The corresponding cyclic voltammograms are illustrated below in figures 2 and 3 accordingly.

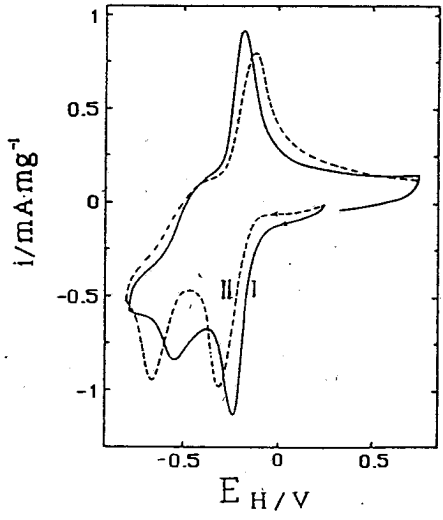

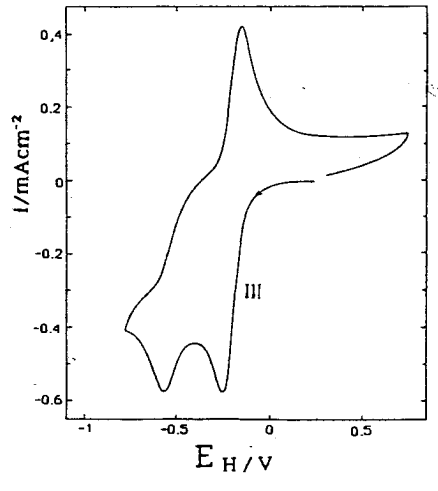

Fig. 2. **Fig. 3.**

Cyclic voltammograms of p-benzoquinone ($5 \cdot 10^{-3}$ M) in PC solution (Et_4NClO_4 0,25 M)
Fig. 2. on platinized carbon fibres (I) and pristine carbon fibres (II) electrodes
Fig. 3. on bulk Pt electrode (III).

From figures 2 and 3 it becomes obvious, that these electrodes cause a small catalytical shift of both reduction steps to more positive potential values (about 100mV). Moreover, the first reduction step is more reversible on both electrodes (platinized carbon fibres and Pt) than on pristine carbon fibres but still not thermodynamically reversible.

The fact that cathodic sweep is cut in two steps is because PC acts as a poor proton donor. To get better oxido-reduction steps of p-benzoquinone we added benzoic acid, as a proton donor, to the solution. Benzoic acid is not ionised in propylene carbonate as the conductometric study has shown; moreover, it has a similar diffusion coefficient such as those of benzoquinone. For these reasons it acts as a real proton donor during the electro-reduction of the nitrocompounds in the interfacial region.By addition of a bimolecular benzoic acid quantity appears one two-electron reversible couple of peaks (Fig. 4) corresponding to the following electrochemical reaction, which is about 500 mV potential catalysed and is strictly diffusion controlled.

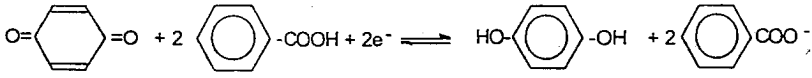

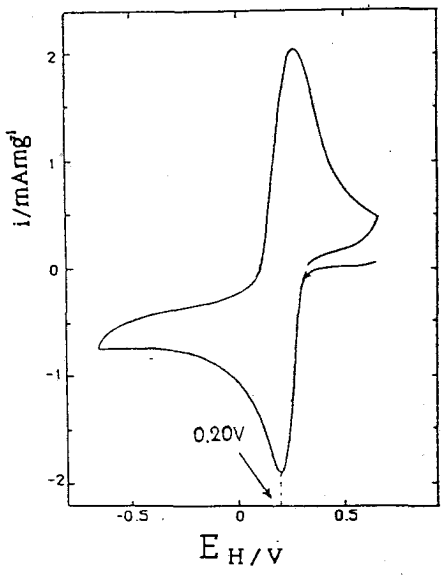

Fig. 4. Cyclic voltammogram of p-benzoquinone ($5 \cdot 10^{-3}$ M) on pristine carbon fibres electrode in PC solution (Et_4NClO_4 0,25 M) in presence of benzoic acid ($2 \times 5 \cdot 10^{-3} = 10^{-2}$ M), v=100 mVsec^{-1}.

The above reversible reaction was further tested on a bulk platinum electrode as well as on platinized carbon fibres. The couple of peaks on both electrodes is reversible; however a slight further shift of the peaks towards more positive values (Fig. 5,6) is observed.

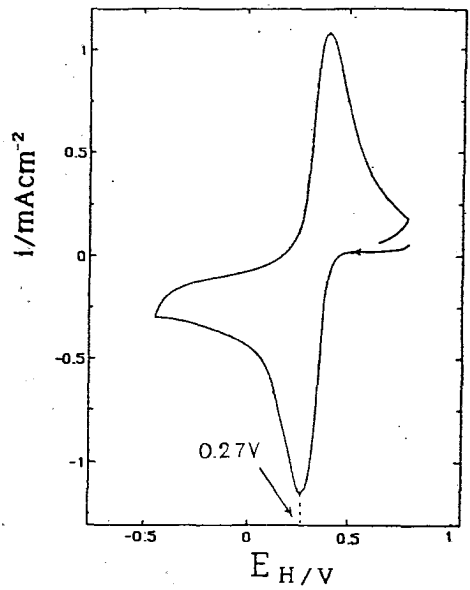

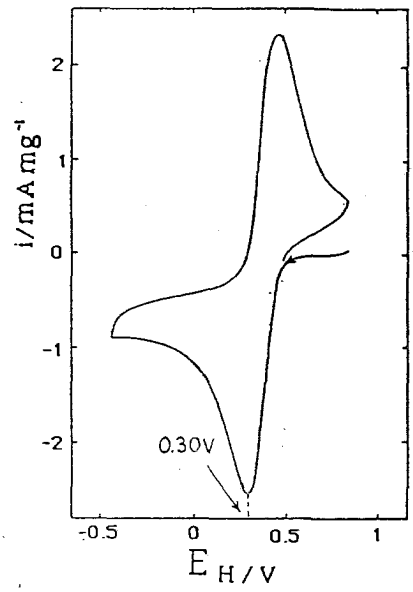

Fig. 5. **Fig. 6.**

Cyclic voltammograms of p-benzoquinone ($5 \cdot 10^{-3}$ M) in PC solution (Et_4NClO_4 0,25 M) in presence of benzoic acid ($2 \times 5 \cdot 10^{-3} = 10^{-2}$ M), v=100 mVsec^{-1}.

Fig. 5. on bulk Pt electrode

Fig. 6. on platinized carbon fibres.

The platinized carbon fibres in PC solutions behave like bulk platinum electrodes, the latter of which needs to be activated and cleared before every use. This behavior has been tested through the catalytic activity of these electrodes on the electro-reduction of p-benzoquinone as can be observed in Fig. 6. in comparison to Fig. 5. The heights of the reversible two-electron step on the platinized carbon fibres is greater than that of the pristine carbon fibres because the surface of the fibres increases due to the fine dispersion of Pt on the fibres. The platinized carbon fibres are very stable and can be stored for long time in PC solutions without losing their mechanical stability and electrocatalytic activity.

With the above data we tried to estimate the electrochemically active surface of the carbon fibres. For this purpose, the electrochemically active surface of the Pt electrode was first estimated by measuring the hydrogen adsorption peak area of the cathodic cyclic voltammetric sweep in 0,1 M H_2SO_4 solutions (Fig. 7) taking into consideration that 210 μCb correspond to 1cm^2 of electrochemically active Pt surface [15,16,17]. The value corresponds to $1{,}3 \cdot 10^{15}$ H atoms per Pt cm^2 and presupposes that every Pt atom of the electrode surface is connected to one H atom. It was so found that the electrochemically active surface of the Pt-electrode used is 10,45mm^2.

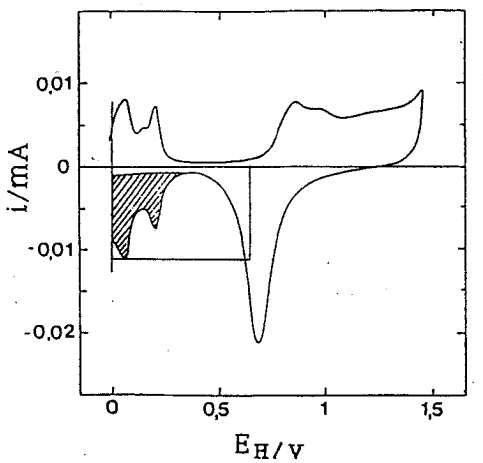

Fig.7. Cyclic voltammogram of H_2SO_4 (0,1 M) on bulk Pt electrode in aqueous solution, v=100 mVsec^{-1}. The adsorption area of hydrogen, which was used to estimate the electrochemically active surface of the Pt-electrode is also indicated.

The i_p of diffusion controlled reversible electrochemical reactions is given by the equation: $i_p=2{,}72\cdot10^5\, n^{3/2}\cdot A\cdot C\cdot D^{1/2}\cdot v^{1/2}$ [18]. Comparing the heights of i_p peaks of p-benzoquinone cyclovoltammograms, in presence of benzoic acid, on pristine carbon fibre electrodes as well as on Pt-electrode and by using the above equation with the known value of the electrochemically active surface of the Pt-electrode, we estimated the electrochemically active surface of the pristine carbon fibres electrode equal to 1,7 cm^2·mg^{-1}.

Conclusion

PAN-based carbon fibre electrodes are convenient for the study of depolarizers in propylene carbonate solutions.

Platinized carbon fibres prepared by simple electrodeposition of platinum on the carbon fibres behave in PC like bulk platinum electrodes. This behavior has been tested through the catalytic activity of these electrodes on the electroreduction of p-benzoquinone.

In presence of a bimolecular quantity of benzoic acid, the p-benzoquinone-p-hydroquinone system is thermodynamically reversible and as a simple redox-system of one bielectronic step it is the ideal one to estimate the electrochemically active surface of solid electrodes in the solvent propylene carbonate which is of great importance for the galvanic cells of lithium as well as for the non-aqueous solvent electrochemistry in general. The commonly used reversible redox-system $Fe(CN)_6^{3-}$ - $Fe(CN)_6^{4-}$ cannot be employed in PC, because the ferro-cyanide salts have a small solubility in this solvent.

ΠΕΡΙΛΗΨΗ

Κυκλοβολταμετρική μελέτη του συστήματος π-βενζοκινόνης - π-υδροκινόνης σε ηλεκτρόδια ινών άνθρακα, ηλεκτρόδια λευκοχρύσου και ηλεκτρόδια επιλευκοχρυσωμένων ινών άνθρακα μέσα σε ανθρακικό προπυλενεστέρα.

Η π-βενζοκινόνη μέσα στον ανθρακικό προπυλενεστέρα (PC) σε ηλεκτρόδια από γραφιτικές ίνες ανάγεται σε δύο σαφώς χωριζόμενες μονοηλεκτρονικές βαθμίδες, γεγονός που αποδίδεται στο ότι το PC είναι πτωχό πρωτικό μέσο. Χρησιμοποιώντας ηλεκτρόδιο λευκοχρύσου ως και ηλεκτρόδια από επιλευκοχρυσωμένες γραφιτικές ίνες οι δυό βαθμίδες αναγωγής της βενζοκινόνης μετατοπίζονται και στις δύο περιπτώσεις προς θετικότερες τιμές δυναμικού.

Με την προσθήκη βενζοϊκού οξέος ως δότη πρωτονίων, σε διπλάσια μοριακή ποσότητα σχετικά με την ποσότητα της π-βενζοκινόνης, η αναγωγή γίνεται σε μία μόνο διηλεκτρονική βαθμίδα, η οποία υπακούει ικανοποιητικά στα κριτήρια των θερμοδυναμικά αντιστρεπτών δράσεων, διέπεται δε από συνθήκες διαχύσεως. Η ηλεκτροχημική αυτή αντίδραση καταλύεται από απόψεως δυναμικού περίπου κατά 500 mV. Το βενζοϊκό οξύ μέσα στο PC δεν υφίσταται ηλεκτρολυτική διάσταση και έχει συντελεστή διαχύσεως περίπου ίσο με αυτόν του αποπολωτή. Έτσι δρα σαν ένας γνήσιος δότης πρωτονίων μέσα στη διαφασική περιοχή.

Η παραπάνω αντιστρεπτή διηλεκτρονική δράση μελετήθηκε σε απλές γραφιτικές ίνες και σε ηλεκτρόδιο λευκοχρύσου του οποίου η ηλεκτροχημικά ενεργή επιφάνεια προσδιορίστηκε με βάση τις χαρακτηριστικές καμπύλες ροφήσεως του υδρογόνου. Για τις ηλεκτροχημικές δράσεις που διέπονται από συνθήκες διαχύσεως και είναι αντιστρεπτές το i_p καθορίζεται από τη γνωστή σχέση: $i_p=2,72\cdot10^5n^{3/2}\cdot A\cdot C\cdot D^{1/2}\cdot v^{1/2}$.

Βάσει της σχέσεως αυτής ο λόγος των υψών των κορυφών i_p στα κυκλοβολταμογραφήματα της μελετούμενης αντιστρεπτής δράσης στα ηλεκτρόδια από γραφιτικές ίνες και στο ηλεκτρόδιο λευκοχρύσου ισούται με το λόγο των ηλεκτροχημικά ενεργών επιφανειών των δύο ηλεκτροδίων. Έτσι, από την ηλεκτροχημικά ενεργή επιφάνεια του ηλεκτροδίου του λευκοχρύσου μπορούμε να προσδιορίσουμε την ηλεκτροχημικά ενεργή επιφάνεια των ηλεκτροδίων από γραφιτικές ίνες.

Επομένως, το σύστημα π-βενζοκινόνης - π-υδροκινόνης παρουσία διμοριακής ποσότητας βενζοϊκού οξέος συμπεριφέρεται ως θερμοδυναμικά αντιστρεπτό και σαν ένα απλό οξειδοαναγωγικό σύστημα μιας διηλεκτρονικής βαθμίδας προσφέρεται για τον προσδιορισμό της ηλεκτροχημικά ενεργού επιφάνειας στερεών ηλεκτροδίων μέσα στο διαλύτη propylene carbonate, ο οποίος έχει ευρεία χρήση στα γαλβανικά στοιχεία

λιθίου και γενικότερα στην ηλεκτροχημεία των άνυδρων διαλυτικών συστημάτων. Το γνωστό οξειδοαναγωγικό σύστημα $Fe(CN)_6^{3-}$ - $Fe(CN)_6^{4-}$ είναι ακατάλληλο στην περίπτωση του PC, διότι τα σιδηροκυανιούχα άλατα είναι πρακτικώς αδιάλυτα μέσα σε αυτό.

LITERATURE

1. J.O. Besenhard und H.P. Fritz, Electrochemische Energietechnik, BMFT 1984,44
2. J.P. Gabano (ed). Lithium Batteries, Academic Press, New York, 1983.
3. E. Theodoridou and D. Jannakoudakis, Z. Naturforsch. 36b (1981) 840.
4. E. Theodoridou, P. Karabinas and D. Jannakoudakis, 37b Z. Naturforsch. (1982) 97.
5. A.D. Jannakoudakis and E. Theodoridou, Z. Phys. Chem. N.F. 129 (1982) 197.
6. P.D. Jannakoudakis and E. Theodoridou, Z. Phys. Chem. N.F. 130 (1982) 49.
7. P.D. Jannakoudakis and E. Theodoridou, Z. Phys. Chem. N.F. 130 (1982) 167.
8. P.D. Jannakoudakis, P. Karabinas and E. Theodoridou, Z. Phys. Chem. N.F. 131 (1982) 89.
9. E. Theodoridou, A.D. Jannakoudakis, Z. Phys. Chem. N.F. 132 (1982) 175.
10. E. Theodoridou, A.D. Jannakoudakis and D. Jannakoudakis, Z. Phys. Chem. N.F. 134 (1983) 227.
11. N. Missaelidis, E. Theodoridou and D. Jannakoudakis, Chim. Chron. N.S. 13 (1984) 45.
12. A.D. Jannakoudakis, C. Tsiamis, P.D. Jannakoudakis, E. Theodoridou, J. Electroanal. Chem. 184 (1985) 123.
13. A.D. Jannakoudakis, E. Theodoridou, D. Jannakoudakis, Synthetic Metals, 10 (1984/85) 131-140.
14. N. Georgolios, D. Jannakoudakis and P.Karabinas, J. Electroanal. Chem. 264 (1989) 235-245.
15. J. S. Bett, K. Kinoshita, K. Routsis and P. Stonehart, J. Catal. 29 (1973) 160.
16. K. Kinoshita, J. Lundquist and P. Stonehart, J. Catal. 31 (1973) 325.
17. Allen J. Bard Electroanalytical Chemistry, Ronald Woods, Vol. 9, 48.
18. A.J. Bard and L.R. Faulkner, Electrochemical Methods, John Wiley and Sons, N.Y. (1980).

Chimika Chronika, New Series, 26, 57-66 (1997)

TANNINS OF EIGHT CAROB VARIETIES FROM THE ISLAND OF LEFKADA, GREECE

S. Marakis[1], G. Marakis[2] and M. Lambraki*[1]

[1]Institute of General Botany, Biology Dept. Athens University, 157 84 Athens, Greece.

[2]Dept. of Food Science and Technology, University of Reading , U.K.

(Received: June 12, 1996 In final form: January 29, 1996)

The total tannin content, tannin qualitative composition, and tannin resistance to microbial activity of eight carob varieties, A-1, A-2, A-3, A-4 (ungrafted) and H-1, H-2, H-3, H-4 (grafted), from Lefkada island, located at the Ionian sea, were studied. The total tannin content of the ripe deseeded carob pod ranges from 4.2 to 6.1% (on pod dry weight). Generally, the ungrafted varieties were richer in tannins than the grafted ones. According to tannin behaviour upon extraction from an aqueous solution with ethyl acetate, carob tannins were generally divided into two groups: i) Sol fraction, passing into the organic phase and ii) Insol-1 and Insol-2 fractions, remaining in the water layer. Tannin analyses showed that carob tannins are mainly condensed. (-) Epigallocatechin, (-) epigallocatechin gallate, (-) epicatechin gallate, delphinidin, cyanidin, pelargonidin, phloroglucinol and gallic acid were detected in all Lefkada's carob varieties. Catechol was generally detected to Lefkada's carob varieties with exception of H-1 and H-4 varieties. Tannins showed a differentiation in resistance to microbial activity depending on the profile of tannins and their relative astrigency value. The higher microbial growth was observed in media containing, as sole carbon source, tannins of H-1 and H-4 varieties.

Key Words: total tannins, tannin fractions, tannin qualitative composition, deseeded carob pod, grafted varieties, ungrafted varieties, epigallocatechin, (-) epigallocatechin gallate, (-) epicatechin gallate, delphinidin, cyanidin, pelargonidin, phloroglucinol, catechol, relative astrigency, resistance to microbial activity.

Introduction

Carob bean is the fruit of *Ceratonia siliqua* L. tree. Carob tree naturally grows on barren and unproductive, for other crops, soils. It occurs in most warm regions of the Mediterranean basin and in other countries (Rhodesia, parts of USA, Australia, South America, India and Philippines) with similar climate to that of the Mediterranean countries [1].

The ripe deseeded carob pod (husk) contains high levels of total tannins, 6-13% for some greek carob varieties [2-5] and 20-27% (on husk dry weight) for carob pods from Portugal, Italy and Cyprus [6].

The main constituents of carob polyphenols were found to be condensed tannins containing the flavan nucleous [3,7,8]

Although the structure of condensed tannins had not been fully investigated, due to the lack of a suitable methodology, some investigators, employing thioglycolic acid to degrade the tannins from common heather (*Calluna vulgaris*) and carob pod, gave a profile of those tannins [3,8,9]. Tamir et al studied the structure of carob condensed tannins but the authors did not mention the carob variety from which tannins were isolated [8]. On the other hand, the tannin profile of nine cretan carob varieties was reported, as well as the significant role of tannin structure against to microbial attack [3].

Since Greece is one of the 80 countries that use *mimosa* tannins for leather tanning and the fourth largest carob producing country in the world, we decided to investigate the possibility, to replace these imported tannins by carob tannins. Trials for using carob tannins for leather tanning are taking place in the Hellenic Centre of Leather (EL.KE.DE) under our supervision.

Thereafter, we continued to study both tannin profile and tannin resistance to microbial attack (activity) of greek carob varieties, other than the cretan ones.

In this paper, tannin profile and tannin resistance to fungal attack of eight carob varieties from Lefkada island are described.

Experimental

Carob bean sampling: Twenty trees from each of the eight recognized varieties [4,5] were chosen from different areas of the greek island of Lefkada located at the Ionian sea. Approximately, 1 kg of carob fruit was collected from different parts of each tree.

After harvesting, the naturally (by sun) dried carob beans were taken to a factory mill where the brittle carob pods were opened and the seeds were separated from the fragments of pod (husk). One kg of carob pods was ground in a mill bearing a 2 mm sieve. The flour obtained was then lyophilized using a freeze-dryer "virtis" [10].

Tannin isolation from ripe carob pod: Tannins were extracted and isolated according to previous procedures [3].

Tannin fractions: The separation of the soluble (Sol) from the insoluble (Insol-1 and Insol-2) fractions in ethyl acetate was carried out by a previous method [11]. The remaining in the water layer Insol-1 and Insol-2 fractions were precipitated by saturated solutions of lead acetate with pH 5.5 and 8.5, respectively.

Tannin hydrolysis by hydrochloric acid: It was carried out by 2 M HCl [3].

Alkaline fusion of tannins: It was performed by the method of Roux [12].

Relative astrigency estimation of the tannins: It was made by the Bate-Smith method, in which relative astrigency was defined as : *the ratio of the concentration of the tannic acid to the concentration of the tannin which cause the same degree of protein precipitation* [13].

Total tannin determination: The total tannins were determined by the Folin-Denis colorimetric method [14].

Tannin detection: It was carried out by RP-HPLC (Millipore - Waters). Standards were purchased from Extrasynthese. Solvents of HPLC grade were purchased from Sigma. A column (25 cm x 4 mm) of LiChrospher 100 RP-18 was used. *Elution:* Two solvents were used: A = 1% aqueous orthophosphoric acid; B = methanol. The elution system was: 0-30 min, 0-15% B in A (linear gradient); 30-45 min, 15-60% B in A (linear gradient); 40-60 min, 60% B in A (isocratic gradient); 60-132 min, 100% B (isocratic gradient); 132-145 min, 100% A (isocratic gradient). Flow rate: 0.5 ml min^{-1}. Wavelength: 240-550 nm.

Culture media of fungi: For the estimation of the fungal growth on substrates containing tannins as sole carbon source, the media A, B and C were used. Medium-A composition (g/l): Freeze-dried tannins of each Lefkada's carob variety = 20, $(NH_4)_2SO_4$ = 5, K_2HPO_4 = 1, $MgSO_4.7H_2O$ = 0.5, KCl = 0.5, $ZnSO_4$ = 0.01, $CuSO_4.5H_2O$ = 0.005, biotin = 0.04, thiamine = 1, pyridoxine hydrochloride = 0.5, and nicotinic acid = 0.5. The pH was adjusted to 4.5 - 5.5. Media-B, C composition: As medium-A, but carob tannins were replaced by (-) epicatechin and catechol (1-2 g/l), respectively.

Microorganisms: Fifty two fungal and yeast strains isolated from natural materials such as carob leaves and fruit, tannery wastes etc. were used [15-18].

Batch cultivation: Fungal cultures were carried out according to our previous paper [17].

Tannase preparation: The purified tannase was prepared from mycelium of *Penicilium glabrum* grown on the tannic acid medium, as it was described by Yamada et al [19]. *P. glabrum* was isolated from young leaves of *C. siliqua* L. [16].

Tannin profile

Tannin HPLC analysis of Lefkada's ripe carob pods showed the presence mainly of condensed tannins (Table III).

Table III. Tannin detection in the ripe husk of eight carob varieties from island of Lefkada, after hydrolysis and alkaline fusion of tannins, sited according to their order of elution from the column. 3-6: Flavanols and their gallic acid esters; 7-9: anthocyanidines; 11-12: phenols of catechol group.

Carob varieties / TANNINS	UNGRAFTED				GRAFTED			
	A-1	A-2	A-3	A-4	H-1	H-2	H-3	H-4
1. Gallic acid	+	+	+	+	+	+	+	+
2. Substance X	+	+	+	+	ND*	ND	ND	ND
3. (-) Epigallocatechin gallate	+	+	+	+	+	+	+	+
4. (-) Epigallocatechin	+	+	+	+	+	+	+	+
5. (-) Epicatechin gallate	+	+	+	+	+	+	+	+
6. (-) Epicatechin	Trace	Trace	Trace	Trace	ND	Trace	Trace	ND
7. Delphinidin	+	+	+	+	+	+	+	+
8. Cyanidin	+	+	+	+	+	+	+	+
9. Pelargonidin	+	+	+	+	+	+	+	+
10. Phloroglucinol	+	+	+	+	+	+	+	+
11. Pyrogallol	+	+	+	+	+	+	+	+
12. Catechol	+	+	+	+	ND	+	+	ND

ND*: Not Detected

(-) Epigallocatechin, (-) epigallocatechin gallate (Figure 1) and (-) epicatechin gallate were detected in all Lefkada's carob varieties. The presence of gallic acid, phloroglucinol and catechol is an additional confirmation for the presence of (-) epicatechin gallate. The presence of gallic acid can also be attributed to hydrolysis of the gallate esters. (-) Epicatechin was absent from the H-1 and H-4 varieties, as it was from u-5 and g-4 cretan varieties, as well [3]. An unidentified tannin (X) was found only in the husk of the ungrafted varieties. This substance, also present in some

cretan carob varieties [3], gave catechin and gallic acid by enzymic (tannase) degradation. As Haslam reported, this phenol sould be catechin-3-gallate [20].

Figure 1. Structure of (-) epigallocatechin and (-) epigallocatechin gallate.

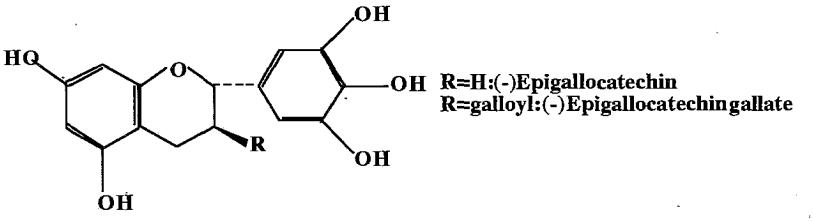

Catechol was generally detected in the Lefkada's carob varieties with exception of the H-1 and H-4 grafted ones. This compound was also found in all cretan varieties studied except g-1 grafted variety [3]. Delphinidin, cyanidin and pelargonidin (anthocyanidines) were identified in all Lefkada's carob varieties. These compounds may be derived by hydrolysis of anthocyanins or from the polymeric catechin, the copolymer of catechin and leucoanthocyanidin or the polymeric leucocyanidin, by the alkaline fusion of them.

Figure 2 shows the HPLC chromatogram of the H-2 carob variety, a common grafted variety of Lefkada island. The flavanols and their gallic acid esters (compounds 3-6) were the first tannins eluted, just before anthocyanidines (compounds 7-9) and phenols of catechol group (compouds 10-12). This latest group represented quantitatively more of the half of all the other compounds. Pyrogallol appeared to be the major phenolic constituent of this variety, 5 fold higher than the average of the rest compounds. With an exception of (-) epigallocatechin gallate, the percentages of the flavanols and their esters with gallic acid were significantly lower compaired with the other compounds eluted.

Flavanols and their gallic acid esters: Generally, the values of these substances, in the ungrafted varieties, were 1.5-2 fold higher than the grafted ones. All the ungrafted varieties presented a similar figure, except A-1 variety, in which the amounts of epigallocatechin gallate, epigallocatechin and epicatechin gallate were twice higher than the same compounds at the chromatograms of the other ungrafted varieties.

Anthocyanidines: These compounds presented a high differentiation among the examined varieties. The lower percentages of this group were found in H-2 varietty.

Results and Discussion

Based on carob bean morphological and chemical characteristics, eight carob varieties from Lefkada island (four ungrafted A-1, A-2, A-3, A-4 and four grafted H-1, H-2, H-3, H-4) were recognized [4,5].

The total tannin content of the ripe deseeded carob pod ranges from 4.2 to 6.1% (on husk dry weight) (Table I).

Table I. Total carob tannins (% on husk dry weight) of eight carob varieties from island of Lefkada. Given numbers are mean values of tannin contents (%) ± s.e., n=6.

Carob	Ungrafted				Grafted			
varieties	A-1	A-2	A-3	A-4	H-1	H-2	H-3	H-4
Tannins	6.1 ± 0.10	5.7 ± 0.05	5.4 ± 0.10	5.6 ± 0.07	4.2 ± 0.10	4.9 ± 0.06	4.7 ± 0.10	4.5 ± 0.20

Generally, the ungrafted varieties are richer in tannins than the grafted ones. This is in agreement with the results previously reported for nine cretan carob varieties [2,3] and probably indicates the protective role of tannins towards the natural "wild" varieties against the microbial attack and the herbivores [17].

According to tannin behaviour upon extraction from an aqueous solution with ethyl acetate, carob tannins were generally divided into two groups: i) Soluble (Sol) fraction, passing into the organic phase and ii) Insoluble (Insol-1, Insol-2) fractions remaining in the water layer. Grafted varieties were generally richer in Insol-1 fraction but poorer in Insol-2 compared to the ungrafted ones (Table II). A similar figure of tannin fractions was reported for the cretan carob varieties [3].

Table II. Tannin fractions (% on total tannin weight) after extraction with ethyl acetate.

	Tannin fractions		
Carob Varieties	Sol Fraction	Insol-1	Insol-2
Grafted	3.5 - 4.1	0.50 - 0.65	0.20 - 0.35
Ungrafted	4.5 - 5.1	0.30 - 0.40	0.55 -0.67

Higher amounts were detected to the other varieties, that gradually reached almost 2.5 folder the amount of H-2 variety. In increasing order: H-2<H-3<H-1<H-4<A-3<A-2<A-4<A-1.

Figure 2. HPLC chromatogram showing the tannin profile of H-2 variety of Lefkada island.

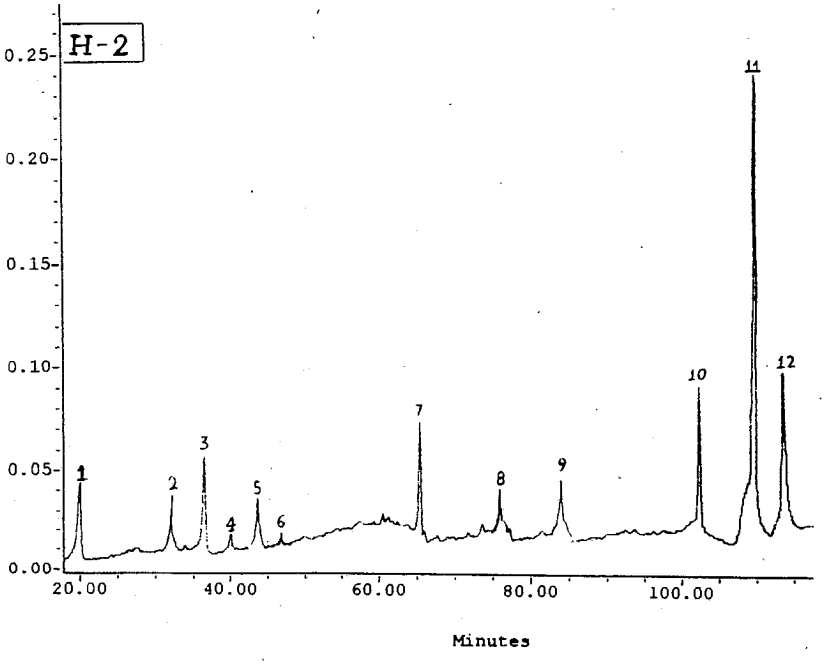

Catechol group: The H-3 variety chromatogram had a similar figure to that of the H-2, concerning the catechol group, while the same group at the H-1 and H-4 varieties was

the 1/3 of the H-2. All the ungrafted varieties presented a similar figure, in quantities slightly less than the H-2 grafted variety.

Gallic acid (compound 1) was significantly present in all the examined varieties.

The results led us to conclude that the qualitative tannin profile of Lefkada's carob varieties present lower differentiation compared to that of cretan carob varieties [3].

Fungal growth

From the microbiological point of view, the tannins of the examined Lefkada's carob varieties showed a differentiation in resistance to microbial attack depending on the carob variety and relative astrigency value. Thus, the growth of 52 fungal and yeast strains was not only poorer in media containing the tannins found in ungrafted varieties, than those of grafted varieties, but also, only a limited number of microorganisms grew in tannins of ungrafted varieties. Particularly, media containing tannins of the H-1 and H-4 varieties supported the growth of most of the microbial strains and showed the most luxuriant growth. This is probably due to the lack of (-) epicatechin, catechol, or of substance X, in these varieties (Table III), as a very poor fungous growth was observed for two strains of filamentous fungi, *Aspergillus carbonarius* and *Penicillium glabrum,* with high tanninolytic ability [18] in the media B and C containing (-) epicatechin and catechol, as sole carbon source, respectively. In addition, the luxuriant fungous growth in tannins of the H-1 and H-4 varieties may be also related with a higher degree of tannin polymerization, than that of other Lefkada's varieties, because the higher degree of polymerization results in the lower relative astrigency [3] and consequently the lower antifungous activity. The relative astrigency values for the different tannin fractions of Lefkada's carob pods are shown at table IV.

Table IV. Relative astrigency values for tannin fractions of different degree of polymerization.

Fraction	Relative astrigency
Dimer	0.09 - 0.10
Trimer	0.28 - 0.32
Tetramer	0.37 - 0.43
Oligomer	0.48 - 0.54

On the base of the above mentioned, we could say that tannins of the H-1 and H-4 varieties should not be suggested for leather tanning. On the contrary, preliminary

experiments using the most common variety in Crete [2], showed that in solid cultures, all the tannin fractions of this variety, are microbially consumed, except of the group of catechols. So, since catechols are used for tanning leather, more trials should be done for finding out if carob catechols have good tanning properties.

ΠΕΡΙΛΗΨΗ

ΤΑΝΝΙΝΕΣ ΧΑΡΟΥΠΑΛΕΥΡΟΥ ΟΚΤΩ ΠΟΙΚΙΛΙΩΝ ΤΗΣ ΝΗΣΟΥ ΛΕΥΚΑΔΑΣ

Προσδιορίσθηκε το ποσοστό των ολικών ταννινών οκτώ ποικιλιών, Α-1, Α-2, Α-3, Α-4 (ανεμβολίαστες) και Η-1, Η-2, Η-3, Η-4 (εμβολιασμένες), της νήσου Λευκάδας, ταυτοποιήθηκαν (HPLC) τα συστατικά τους, μετά από όξινη υδρόλυση και αλκαλική σύντηξη και μελετήθηκε, η αντοχή τους στη μικροβιακή δραστηριότητα. Η επί τοις % περιεκτικότητα του χαρουπάλευρου σε ολικές ταννίνες κυμάνθηκε από 4.2 έως 6.1% (επί ξηρού χαρουπάλευρου). Γενικά, το χαρουπάλευρο των ανεμβολίαστων ποικιλιών ήταν πλουσιότερο σε ταννίνες σε σχέση με το χαρουπάλευρο των εμβολιασμένων. Ανάλογα με τη συμπεριφορά των ταννινών κατά την εκχύλισή τους με υδατικό διάλυμα οξικού αιθυλεστέρα διακρίναμε δύο ομάδες: i) το διαλυτό (Sol) κλάσμα, το οποίο περνά στην οργανική φάση και ii) τα αδιάλυτα (Insol-1, Insol-2) κλάσματα, τα οποία παραμένουν στην υδατική φάση. Η ανάλυση της δομής των ταννινών στο χαρουπάλευρο όλων των Λευκαδίτικων ποικιλιών έδειξε ότι οι φαινολικές αυτές ενώσεις ανήκουν στην ομάδα των συμπυκνωμένων ταννινών όπως η (-) επιγαλλοκατεχίνη, (-) επιγαλλοκατεχίνη γαλλική, (-) επικατεχίνη γαλλική και των ανθοκυανιδινών όπως η δελφινιδίνη, κυανιδίνη, πελαργονιδίνη. Επίσης ταυτοποιήθηκαν οι φαινόλες φλωρογλυκινόλη, πυρογαλλόλη και κατεχόλη (η τελευταία με εξαίρεση στις ποικιλίες Η-1 και Η-4) και γαλλικό οξύ. Η αντοχή των ταννινών έναντι της μικροβιακής δραστηριότητας, βρέθηκε διαφοροποιούμενη ανάλογα με τη σύσταση και τη σχετική στυπτικότητά των ταννινών. Η υψηλότερη μικροβιακή αύξηση παρατηρήθηκε στα θρεπτικά μέσα, τα οποία, ως μόνη πηγή άνθρακα, περιείχαν ταννίνες των ποικιλιών Η-1 και Η-4.

References

1. Marakis, S. Biotechnol. Lett. 1995, 14, 1075-1080.
2. Marakis, S.; Kalaitzakis, J.; Mitrakos K. In: FITO P. and MULET A., Proc. of IInd Int. Carob Symp., Spain, Valencia, 29 Sept. - 1 Oct., 1987; pp. 195-208 .
3. Marakis, S.; Lambrakis, M.; Diamantoglou, S. Chimica Chronica, New Series 1993, 22, 213-224.
4. Gaitis, F.; Marakis, S.; Diamantoglou, S. In: Proc. of 16th Scientific Symposium of the Hellenic Society of Biological Sciences, Volos, Greece, 5-7 May, 1995; pp. 2.41-2.42.
5. Marakis, S. unpublished data.
6. Würsch, P. In: FITO P. and MULET A., Proc. of IInd Int. Carob Symp., Spain, Valencia, 29 Sept. - 1 Oct. 1987; pp. 621-629.
7. Nachtomi, E.; Alumot, E. J. Sci. Food Agric. 1963, 14, 464-468.
8. Tamir, M.; Nachtomi, E.; Alumot, E. Phytochemistry, 1971, 10, 2769-2774.
9. Betts, M.J.; Brown, B.R., Brown, P.E.; Pike, W.T. Chem. Commun., 1967, 1110-1112.
10. Marakis, S. Ph. D. Thesis, Univ. of Athens, 1980 (in greek with summary in English).
11. Roux, D.G. J. Amer. Leather Chem. Ass., 1958, 53, 384-395.
12. Vuataz, L.; Brandenberger, H; Egli R.H. J. Chromatography, 1959, 2, 173-187.
13. Bate-Smith, E.C. Phytochemistry, 1973, 12, 907-912.
14. AOAC (1970). Official Methods of Analysis of the Association of Official Agricultural Chemists, 11th ed., Washington, Horwitz W. Ed.
15. Charpentie, M.J.; Marakis, S. Crypt. Mycologie, 1980, 1, 165-174.
16. Marakis, S.; Karagouni, A. Biotechnol. Lett. 1985, 7, 831-836.
17. Marakis, S.; Diamantoglou, S. Crypt. Mycologie, 1990, 11(4), 243-254.
18. Marakis, S. Crypt. Mycologie, 1995, 16(2), 111-119.
19. Yamada, H.; Adachi, O.; Watanabe, M.; Sato, N. Agric. Biol. Chem., 1968, 32, 1070-1078.
20. Haslam, E. J. Chem. Soc. 1969, (C): 1824-1828.

CONTENTS

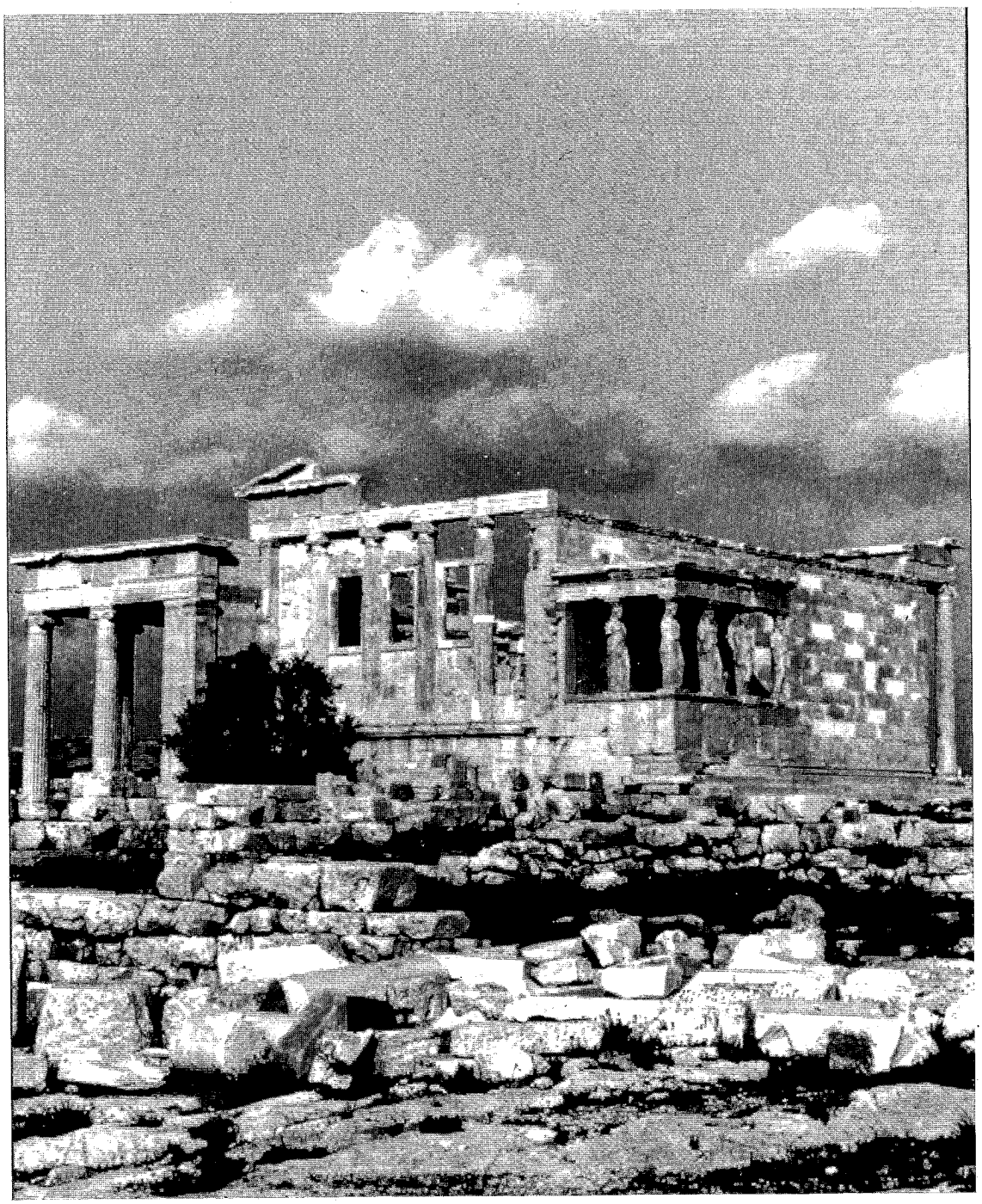

ΟΛΥΜΠΙΑΚΗ ΑΕΡΟΠΟΡΙΑ

ΕΡΕΧΘΕΙΟΝ

ΕΛΛΗΝΙΚΟΣ ΟΡΓΑΝΙΣΜΟΣ ΤΟΥΡΙΣΜΟΥ